Title

Somatic LINE-1 retrotransposition in cortical neurons of Rett patients and healthy individuals

Authors and Affiliations

Boxun Zhao[1,2], Qixi Wu[3,4], Adam Yongxin Ye[4,5,6], Jing Guo[1,7], Xianing Zheng[1,2], Xiaoxu Yang[5], Linlin Yan[5], Qing-Rong Liu[8], Thomas M. Hyde[9,10], Liping Wei[1,2,5,*], August Yue Huang[5,*]

1 National Institute of Biological Sciences, Beijing, 102206, China

2 Graduate School of Peking Union Medical College, Beijing, 100730, China

3 School of Life Sciences, Peking University, Beijing, 100871, China

4 Peking-Tsinghua Center for Life Sciences, Beijing, 100871, China

5 Center for Bioinformatics, State Key Laboratory of Protein and Plant Gene Research, School of Life Sciences, Peking University, Beijing, 100871, China

6 Academy for Advanced Interdisciplinary Studies, Peking University, Beijing, 100871, China

7 College of Life Sciences, Beijing Normal University, Beijing, 100875, China

8 Laboratory of Clinical Investigation, National Institute on Aging, Baltimore, MD 21224, USA

9 Lieber Institute for Brain Development, Baltimore, MD 21205, USA

10 Departments of Psychiatry & Behavioral Sciences and Neurology, Johns Hopkins University School of Medicine, Baltimore, MD 21205, USA

*Correspondence

Correspondence should be addressed to A.Y.H. (huangy@mail.cbi.pku.edu.cn) and L.W.

(weilp@mail.cbi.pku.edu.cn).

Short title

Somatic L1 mosaicism in Rett and healthy individuals

Keywords

mosaicism, retrotransposition, somatic insertion, Rett syndrome

Abstract

Mounting evidence supports that LINE-1 (L1) retrotransposition can occur postzygotically in healthy and diseased human tissues, contributing to genomic mosaicism in the brain and other somatic tissues of an individual. However, the genomic distribution of somatic L1Hs (Human-specific LINE-1) insertions and their potential impact on carrier cells remain unclear. Here, using a PCR-based targeted bulk sequencing approach, we profiled 9,181 somatic insertions from 20 postmortem tissues from five Rett patients and their matched healthy controls. We identified and validated somatic L1Hs insertions in both cortical neurons and non-brain tissues. In Rett patients, somatic insertions were significantly depleted in exons—mainly contributed by long genes—than healthy controls, implying that cells carrying *MECP2* mutations might be defenseless against a second exonic L1Hs insertion. We observed a significant increase of somatic L1Hs insertions in the brain compared with non-brain tissues from the same individual. Compared to germline insertions, somatic insertions were less sense-depleted to transcripts, indicating that they underwent weaker selective pressure on the orientation of insertion. Our observations demonstrate that somatic L1Hs insertions contribute to genomic diversity and MECP2 dysfunction alters their genomic patterns in Rett patients.

Author Summary

Human-specific LINE-1 (L1Hs) is the most active autonomous retrotransposon family in the human genome. Mounting evidence supports that L1Hs retrotransposition occurs postzygotically in the human brain cells, contributing to neuronal genomic diversity, but the extent of L1Hs-driven mosaicism in the brain is debated. In this study, we profiled genome-wide L1Hs insertions among 20 postmortem tissues from Rett patients and matched controls. We identified and validated somatic L1Hs insertions in both cortical neurons and non-brain tissues, with a higher jumping activity in the brain. We further found that MECP2 dysfunction might alter the genomic pattern of somatic L1Hs in Rett patients.

Introduction

The term "somatic mosaicism" describes the genomic variations that occur in the somatic cells that make up the body of an individual. These variations contribute to intra-individual genetic diversity among different cells (Campbell et al., 2015). In addition to various types of cancers, somatic mosaicisms reportedly contribute to a variety of neurological disorders, including epilepsy, neurodegeneration, and hemimegalencephaly (Poduri et al., 2013). The human-specific LINE-1 (L1Hs) retrotransposon family is the only known family of active autonomous transposons in the human genome (Hancks and Kazazian, 2012; Kazazian and Moran, 2017). L1s retrotranspose through a process called target-primed reverse transcription (TPRT), with the capacity for *de novo* insertion into new genomic locations in both germline and somatic cells (Cost et al., 2002; Luan et al., 1993). Mounting evidence supports that L1Hs elements, with increased copy number in the brain relative to

other tissues, contribute to neuronal diversity via somatic retrotransposition (Coufal et al., 2009; Erwin et al., 2016; Evrony et al., 2012; Evrony et al., 2015; Muotri et al., 2010; Upton et al., 2015).

Recent studies reported the occurrence of somatic L1Hs insertions during neurogenesis and in non-dividing mature neurons (Coufal et al., 2009; Macia et al., 2017). Other studies have observed dysregulated L1Hs copy number in patients with Rett syndrome (Muotri et al., 2010) and schizophrenia (Bundo et al., 2014). Methyl-CpG binding protein 2 (*MECP2*) is the major disease-causing gene of Rett syndrome (Amir et al., 1999). Its gene product, MeCP2, can bind to the 5' UTR of L1 elements and represses their expression and retrotransposition (Yu et al., 2001). While it is known that L1 expression and copy number are elevated in the brains of *Mecp2* knockout mice as well as in patients with Rett syndrome (Muotri et al., 2010; Skene et al., 2010), little is known about the genomic distribution patterns of somatic L1Hs insertions in Rett patients and healthy individuals.

In contrast to germline insertions, the effects of somatic transposon insertions depend not only on their genomic location. Rather, the specific timing, tissue, and cell lineage at which they occur profoundly influence the impact of somatic insertions (Frank, 2010). Single-cell targeted sequencing approaches have been used to identify somatic insertions (Erwin et al., 2016; Evrony et al., 2012; Upton et al., 2015). However, such methods typically require a large number of cells and demand considerable sequencing depth for unbiased profiling of human tissues (Grun and van Oudenaarden, 2015; Navin, 2015). Furthermore, owing to the rarity of somatic insertions, investigations of the clonal diversity of somatic insertions would require the sequencing of even larger numbers of cells (Navin, 2015).

Another limitation of single-cell sequencing approaches is that errors of allelic dropout and locus dropout, which frequently occur during the whole genome amplification (WGA) step of library construction, can reduce the sensitivity and specificity of somatic insertion detection. Estimates of the rate of somatic L1Hs insertions vary widely in single-cell genomics studies (Faulkner and Garcia-Perez, 2017). Bulk sequencing approach can potentially overcome these limitations and enable the genome-wide identification and quantification of somatic L1Hs insertions, but their low allele frequency in cell populations poses a great challenge to distinguishing true insertion events from technical artifacts (Evrony et al., 2016).

Here, we introduced a PCR-based multiplex bulk sequencing method for sensitive enrichment and specific identification of L1Hs insertions from various types of human tissues. We used this method to perform genome-wide L1Hs insertion profiling of 20 postmortem tissues from five patients with Rett syndrome and their matched healthy controls. The aims of this study were to explore the genomic patterns of somatic L1Hs insertions in neuronal and non-neuronal samples, and to investigate whether MECP2 dysfunction could alter the distribution of L1Hs retrotransposition in patients with Rett syndrome.

Results

A bulk sequencing method to identify L1Hs insertions

Systematic genome-wide profiling of somatic L1Hs insertions requires effective enrichment of

insertion signals and specific identification of true signals from background noise. Enriching neuronal nuclei from bulk brain tissue facilitates the accurate deciphering of cell type-specific characteristic and increases the chance of identifying clonal somatic insertions that are derived from the same progenitor cell and shared by multiple neurons. Therefore, we labeled prefrontal cortex (PFC) neuronal nuclei using an antibody against neuron-specific marker NeuN (Mullen et al., 1992), and subsequently purified $NeuN^+$ nuclei from postmortem human PFC by fluorescence-activated cell sorting (FACS) (Fig 1A; S1A–D Fig; Appendix 1). All initially sorted nuclei were re-analyzed with a second round of FACS, and the purity of the initial sorting was found to be > 96% (S1E–F Fig; Appendix 1). The integrity and purity of sorted nuclei were confirmed by fluorescence microscopy (S2A–C Fig).

To distinguish the signals of active L1Hs elements from other transposon families that are typically inactive in human, we developed a method called human active transposon sequencing (HAT-seq) (Fig 1B; S3A Fig; S1 Table) based on ATLAS (Badge et al., 2003) and several versions of high-throughput sequencing-based L1 amplification methods (Erwin et al., 2016; Ewing and Kazazian, 2010; Philippe and Cristofari, 2016; Tang et al., 2017). Firstly, L1Hs insertions were specifically enriched and amplified using a primer targeting the diagnostic “AC” motif of L1Hs (Hancks and Kazazian, 2012; Ovchinnikov et al., 2001). To ameliorate the poor performance of Illumina sequencing platform for low-diversity libraries, we employed a nucleotides-shifting design by adding two, four, or six random nucleotides upstream of the L1Hs-specific primer, which greatly increased the diversity of the structure-transformed semi-amplicon library and markedly improved the sequencing quality of L1Hs 3’ end. The constructed libraries preserved information regarding the insertion direction and were

sequenced by multiplexed 150 bp paired-end reads. This approach provided sequence information fully spanning the 3' L1Hs-genome junction of each of L1Hs insertions, which enabled the identification of integration sites and facilitated *in silico* false-positive filtering based on both sequence features and read-count.

Genomic position of each L1Hs insertion was determined by the alignment of its 3' flanking sequence (Fig 1C). A custom data analysis pipeline classified putative insertions into one of the following four categories: known reference (KR) germline insertions, known non-reference (KNR) germline insertions, unknown (UNK) germline insertions, and putative somatic insertions (S3B Fig). To further remove technical artifacts induced by non-specific or chimeric amplification and read misalignment in next-generation sequencing, we designed a series of stringent error filters to remove them in different aspects (Table 1): 1) read pairs with non-specific amplification signals and incorrect 3' truncation were removed based on the sequence of L1Hs 3' end (Read 2); 2) after merging paired-end reads into contigs, chimeric molecules with abnormal contig structures were identified by BLAST and filtered out; 3) reads with inconsistencies in BWA-MEM and BLAT alignments were defined as mapping errors; and 4) putative somatic insertion signals without multiple PCR duplicates or those present in different individuals were removed, as they were deemed likely to have resulted from sequencing errors. After applying these error filters, the remaining insertions were annotated with peak features to facilitate downstream analysis.

143 **Table 1. Error filters used in the computational pipeline.**

Filter name	Definition
Improper alignment	We rejected reads with less than 30-bp alignment or more than 3 mismatches to the reference genome.
Diagnostic motif	We rejected reads without L1Hs diagnostic G motif (position 6012 relative to the L1Hs Repbase consensus) (Bao et al., 2015).
Chimera within L1 segment	We rejected reads with less than 95% identity (> 4 mismatches) to the L1Hs 3' end consensus sequence.
Chimera within poly-A tail	We rejected reads at risk of being chimeric (Upton et al., 2015). Read was re-aligned to hg19 using BLAST to find the corresponding best alignments for the non-retrotransposon and retrotransposon segments. Read was removed as a putative chimera when the overlap of the two best segments was > 10 bp and A% ≥ 50% or 6–10 bp and A% < 50%.
Subfamily filter	We rejected putative somatic insertion sites that overlapped with L1 young subfamilies (L1Hs and L1PA2–4) reference insertions.
Known non-reference filter	We rejected putative somatic insertion sites that overlapped with known non-reference L1 insertions in eul1db (Mir et al., 2015).
Misaligned reads	We rejected reads at risk of being misaligned, defined as inconsistent BWA and BLAT alignment.
Local SV	We rejected reads at risk of being derived from a nearby reference L1Hs (Upton et al., 2015). We extracted 2 kb from the reference genome extending downstream from an aligned non-retrotransposon section and aligned the full read contig against this region with BLAT to exclude genomic rearrangements.
Observed in common	We rejected putative somatic insertion sites observed in two or more individuals.
PCR duplicate	We rejected somatic insertion sites without supporting PCR duplicates.

144

145 **Performance evaluation of the HAT-seq method using a positive control**

146 To benchmark the performance of HAT-seq for detecting somatic L1Hs insertions, we experimentally
147 generated a series of positive control samples with insertions at different frequencies by mixing the
148 genomic DNA (gDNA) extracted from the blood samples of two unrelated adults, ACC1 and ACC2
149 (see details in Materials and Methods). 172 ACC1 non-reference germline L1Hs insertions were
150 identified by HAT-seq, 64 of which were confirmed to be ACC1-specific by 3' junction PCR (3' PCR)
151 analysis of gDNA from ACC1 and ACC2 (Fig 2A; S2 Table; Appendix 2) and thus served as positive
152 controls. Three HAT-seq libraries were generated from samples consisting of ACC2 gDNA spiked with
153 1%, 0.1%, or 0.01% of ACC1 gDNA. Considering that decreasing the number of cells pooled for
154 sequencing increased the signal-to-noise ratio for detecting somatic insertions (Evrony et al., 2016),
155 each HAT-seq library was constructed from 20 ng input (about 3,000 cells).
156
157 The zygosity of ACC1-specific L1Hs insertions was confirmed by full-length PCR: 49 of which were
158 heterozygous, 9 of which were homozygous, and 6 of which were zygosity-undetermined (Fig 2B; S2
159 Table; Appendix 2). We detected all 64 ACC1-specific insertions in our positive control 1% ACC1
160 spike-in library, 49 (76.6%) of which passed all of error filters and subsequently were deemed
161 "identified" by HAT-seq. In the 0.1% library, we detected 23 ACC1-specific insertions (16
162 heterozygous, 4 homozygous, and 3 zygosity-undetermined), 17 (73.9%) of which were identified. In
163 the 0.01% library, we detected seven heterozygous ACC1-specific insertions, five (71.4%) of which
164 were identified. The distributions of signal counts (reads with unique start positions) per ACC1-
165 specific insertion followed the Poisson distribution (Fig 2C), indicating a similar probability for each

166 of ACC1-specific insertions to be randomly sampled. In the 1%, 0.1%, and 0.01% libraries, each of
167 ACC1-specific insertions was diluted to 30, 3, and 0.3 copies. Theoretically, by Poisson statistics, there
168 would be 64, 60.81, and 16.59 ACC1-specific insertions being sampled and subsequently being used
169 as the input of HAT-seq libraries (see details in Materials and Methods). Therefore, we estimated the
170 sensitivity of HAT-seq for somatic L1Hs insertions in 1%, 0.1%, and 0.01% libraries as 76.6% (49/64),
171 28% (17/60.81), and 30.1% (5/16.59), respectively. Our data showed that, with about 3,000 cells as
172 input, HAT-seq was able to detect somatic insertion events present in a single cell (Fig 2D and
173 Appendix 3).
174
175 To further evaluate the efficacy of our L1Hs identification pipeline, we compared the proportions of
176 true positives and false positives after applying all the error filters. For the most stringent evaluation,
177 only those 64 ACC1-specific germline insertions in spike-in libraries were defined as “true positives”;
178 all other signals were defined as “false positives”, which might include both background noise and
179 some true somatic insertions present in the blood gDNA. As shown in Fig 2E, in three positive control
180 experiments with 1%, 0.1%, and 0.01% ACC1 gDNA spike-in, 76.56%, 73.91%, and 71.43% of true
181 positives remained after all filters, whereas only 3.40% (66), 6.90% (181), and 7.70% (183) of false
182 positives remained after all filters (S3 Table). These results showed that HAT-seq performed in
183 combination with our error filters could successfully remove most artifacts and identify very low-
184 frequency somatic insertions in bulk DNA samples.
185

186 **Profiling of somatic L1Hs insertions in brain and non-brain human tissues**

187 Next, we applied HAT-seq to 20 bulk samples obtained from postmortem neuronal (PFC neurons) and
188 non-neuronal tissues (heart, eye, or fibroblast) from five Rett syndrome patients and five
189 neurologically normal age-, gender-, and race-matched controls (Table 2 and S4–S7 Table). A total of
190 9,181 putative somatic L1Hs insertions were identified in these 20 HAT-seq libraries (S8 Table). A
191 subset of 137 (1.49%) of these insertions were detected by reads with multiple start positions.
192 Considering that the random fragmentation process in HAT-seq library preparation would result in only
193 one start position shared by all reads generated from a single cell, these 137 insertions should be present
194 in multiple cells in the bulk tissue, and thus classified as "clonal somatic insertions". Based on the
195 performance evaluation of HAT-seq, the lower bound of the precision of overall somatic L1Hs
196 insertions was 60.14%. To demonstrate the validity of these identified somatic insertions *in silico*, we
197 investigated whether they had the hallmark features of TPRT-mediated retrotransposition (see details
198 in Materials and Methods). By exploiting the sequence information of L1 integration junctions, we
199 found that such somatic insertions were significantly enriched in genomic regions containing L1
200 endonuclease cleavage motifs (L1 EN motifs) ($p < 2.2\times10^{-16}$, Wilcoxon rank–sum test; Fig 3A; S4
201 Figu; S9 Table). Moreover, our identified somatic insertions shared the 25-bp peak of poly-A tail length
202 with the reference L1Hs insertions (Fig 3B and S9 Table), where some of the somatic insertions with
203 shorter tails might be explained by non-TPRT mechanism (Morrish et al., 2002). These features of
204 somatic L1Hs insertions helped to elucidate the specificity of HAT-seq method.

05 **Table 2. Overview of postmortem human tissues.**

UMB ID[a]	Category	Mutation	Age	PMI	Brain tissue	Non-brain tissue	Matched ID	Number of somatic insertions		Rate of somatic insertions per cell		Known reference insertions (KRs)	Known non-reference insertions (KNRs)	Unknown insertions (UNKs)
								Cortical neuron	Non-brain	Cortical neuron	Non-brain			
4882	Rett syndrome	c.763C>T (p.R255X)	17 years 310 days	18 hours	PFC	Heart	4591	855	364	1.47	1.01	819	194	10
1815	Rett syndrome	IVS3-2 A>G	18 years 130 days	5 hours	PFC	Eye	1571	589	306	1.30	0.68	806	189	11
4852	Rett syndrome	c.451G>T (p.D151Y)	19 years 280 days	13 hours	PFC	Eye	1347	380	257	0.89	0.54	824	171	8
4516	Rett syndrome	c.763C>T (p.R255X) [b]	20 years 356 days	9 hours	PFC	Fibro blast	1846	759	411	1.82	0.69	814	195	7
1420	Rett syndrome	No pathogenic mutations	21 years 22 days	18 hours	PFC	Heart	1455	708	216	1.31	0.37	824	182	8
4591	Healthy control	NA	16 years 223 days	14 hours	PFC	Heart	4882	861	190	1.58	0.34	816	187	12
1571	Healthy control	NA	18 years 138 days	8 hours	PFC	Heart	1815	384	221	0.63	0.57	813	175	11
1347	Healthy control	NA	19 years 76 days	16 hours	PFC	Heart	4852	553	260	1.08	0.72	806	179	12
1846	Healthy control	NA	20 years 221 days	9 hours	PFC	Heart	4516	744	296	1.66	0.68	817	175	8
1455	Healthy control	NA	25 years 149 days	7 hours	PFC	Heart	1420	628	203	1.16	0.41	802	183	11

06 [a] The gender and race for all individuals were female and Caucasian. [b] Genetic variant identified by custom AmpliSeq capture panel (S4 Table).

207 Owing to the rarity of each somatic insertion in the cell population and to the sensitivity limits of
208 various analytical methods, experimental validation of somatic insertions using unamplified bulk DNA,
209 in particular when one of the primers is complementary to numerous homologous sequences in the
210 human genome is very challenging (Appendix 4). In theory, if a somatic insertion was unique to a
211 single cell, it would be impossible to detect it in any replicated gDNA extracted from the same tissue.
212 To circumvent this, we performed single-copy cloning by adapting a modified version of digital nested
213 3' PCR (Evrony et al., 2015) that focused exclusively on clonal somatic insertions with three or more
214 supporting signals, whose mosaicism (percentage of cells) were at least 0.1% based on our
215 experimental design of HAT-seq library (Figure 3C). Five out of eight (62.5%) such clonal insertion
216 sites were confirmed via 3' nested PCR and Sanger sequencing of cloned amplification products (Fig
217 3D–H and S10 Table). Four of these clonal somatic insertions were located in introns of *TGM6*, *CNTN4*,
218 *DIP2C*, and *DGKB*; three were sense-oriented to transcripts. To our knowledge, no somatic insertions
219 in non-brain tissues of healthy individuals has been reported (Faulkner and Billon, 2018). We identified
220 and experimentally validated a heart-specific somatic L1Hs insertion from healthy individual
221 UMB#1571 (Fig 3D). Leveraging both the 3' and 5' junctions of somatic L1Hs insertions enable us to
222 characterize the terminal site duplications (TSDs) and L1 endonuclease cleavage site of insertion.
223 Because most of somatic L1Hs insertions were 5' truncated with varied lengths, we screened and
224 selected 22 high-quality step-wise primers covering the full-length L1Hs elements to capture their
225 5' junction. (S11 Table and Appendix 4). Using 5' junction nested PCR, we successfully re-captured
226 and Sanger sequenced the 5' junction of the heart-specific L1Hs insertion in healthy individual
227 (UMB#1571) (Fig 4A and S11 Table). We confirmed this insertion was a full-length somatic L1Hs
228 insertion with 14 bp TSD and a cleavage site at 5'–TT/AAAG–3', similar to the consensus L1 EN

motif 5'–TT/AAAA–3' (Fig 4B–D). Notably, we also validated this 5' junction by combining full-length PCR with 5' junction PCR (Fig 4E and S5E Fig; see details in Materials and Methods).

In addition, we verified one fibroblast- and another heart-specific L1Hs insertion in two patients with Rett syndrome (Fig 3E–F). The heart-specific L1Hs insertion in Rett patient (UMB#1420) was further resolved to be a highly 5' truncated L1Hs insertion (~800 bp) with 9 bp TSD and a cleavage site at 5'–TT/TAAA–3' (S5A–D Fig and S11 Table). The poly-A tails of these two clonal somatic insertions were experimentally measured to be polymorphic, indicating that they may involve multiple mutations after the original somatic retrotransposition events. (Fig 3I and S10 Table). As previously reported (Evrony et al., 2015; Grandi et al., 2013), poly-A tail was shown to be a highly mutable sequence element and might undergo secondary mutations in descendant cells. Furthermore, we confirmed two additional somatic L1Hs insertions from Rett patient UMB#4516 were present in both PFC neurons, PFC glia, and fibroblasts (Fig 3G–H and S7A Fig), suggesting that they might retrotranspose during early embryonic development. Notably, we confirmed the intronic somatic insertion (chr20:2392172) in *TGM6* was a full-length L1Hs insertion with 15 bp TSD and a cleavage site at 5'–AT/AAAA–3' (S6A–D Fig and S11 Table). We further quantified the allele fractions of this insertion using custom droplet digital PCR (ddPCR) assay and found that 6.34% of fibroblasts and 2.87% of PFC neurons contained this L1Hs insertion (S8A–E Fig and S10 Table). Our observations demonstrated that endogenous L1Hs could retrotranspose in various types of non-brain tissues during human development.

249 **Abnormal L1Hs mobilization in patients with Rett syndrome**

250 Our HAT-seq bulk sequencing data enabled us to perform statistical analysis of the exonic and intronic
251 patterns of somatic L1Hs insertions in samples from Rett patients and matched healthy controls. We
252 found 180 somatic insertions that were integrated into exonic regions: 9 of which were located in 5'
253 UTR, 102 of which were located in coding regions, and 69 of which were located in 3' UTR (S12
254 Table). While no significant difference was observed in introns (OR = 0.97, p = 0.44, Fisher's exact
255 test), somatic insertions were significantly depleted in exons (OR = 0.59, $p = 6.6\times10^{-4}$, Fisher's exact
256 test) of Rett patients compared with matched healthy controls (Fig 5A and S13 Table). Previous studies
257 have shown that dysregulation of long genes (> 100 kb) was linked to neurological disorders, including
258 Rett syndrome (Gabel et al., 2015) and autism spectrum disorder (King et al., 2013). We used our HAT-
259 seq data to investigate somatic insertional bias in both long (> 100 kb) and short genes (< 100 kb) of
260 Rett patients. As a result, we found significant depletion of somatic insertions in exons of long genes
261 (OR = 0.27, $p = 5.2\times10^{-5}$, Fisher's exact test) but not short genes (OR = 0.76, p = 0.12, Fisher's exact
262 test; Fig 5B and S13 Table). Our speculation was that if an L1Hs inserted into the exonic regions,
263 especially in important genes, of the *MECP2* mutated cell, the cell would have a higher risk of death
264 and subsequently be cleared up; therefore, the observed exonic depletion of L1 insertions in Rett
265 patients might be resulted from the negative selection acting on those "lethal" exonic insertions.
266
267 In contrast to germline insertions, the impact of somatic insertions depends not only on their genomic
268 location, but also the number of cells carrying that insertion, highlighting the importance of clonal
269 somatic insertions. We found that in cortical neurons of Rett patients, clonal somatic insertions were
270 enriched in introns (OR = 1.85, p = 0.029, Fisher's exact test; Fig 5C and S13 Table); these clonal

intronic insertions were significantly enriched in the sense orientation to the transcripts (OR = 3.3, p = 0.0067, Fisher's exact test; Fig 5D and S13 Table). The presence of L1 insertion in the sense orientation has been reported to interfere with transcriptional elongation of co-localized genes (Han et al., 2004). Considering that clonal insertions are more likely to have occurred at an early stage of development and thus affect a relatively large proportion of cells, these distinct insertion pattern in cortical neurons of Rett patients might indicate potential transcriptional burden on the nervous system.

Genomic patterns of somatic and germline L1Hs insertions

The design of HAT-seq method allowed for unbiased enrichment of both somatic and germline L1Hs insertions from each of bulk DNA samples. As germline insertion had constant genomic copy number in all tissues from the same donor, we used germline insertion as endogenous control to measure the relative copy number of genome-wide somatic insertions in the brain and non-brain tissues. We quantified the relative somatic L1Hs content by calculating the L1Hs-derived read count ratio of somatic to germline insertions using HAT-seq data of each sample (S14 Table; see details in Materials and Methods). Among all Rett patients and their matched controls, we observed a significant increase in the copy number of somatic L1Hs insertions in PFC neurons relative to matched non-brain tissues (heart, eye, or fibroblast) from the same donor ($n = 10$, $p = 2.7\times10^{-4}$, paired *t*-test; Fig 6A and S8F–G Fig). We also estimated the occurrence rate of somatic L1Hs insertions based on the germline insertion copy number of each individual (Fig 6B). This produced an average of 1.29 [95% CI: 1.03–1.55] somatic insertions per PFC neuron versus 0.60 [95% CI: 0.46–0.74] insertions per non-brain cell (S14 Table). Our observation of higher somatic L1Hs rate in PFC neurons from healthy individuals argued

292 for the active retrotransposition of L1Hs in the human brain (Coufal et al., 2009). One significant
293 advantage of HAT-seq was the ability to distinguish signals of somatic insertions from the
294 overwhelming copies of germline L1Hs insertions in the genome (see details in Materials and
295 Methods). Inconsistent with the previous qPCR result (Muotri et al., 2010), when comparing the group
296 of Rett patients with matched healthy controls, we only observed a slight but not significant increase
297 of somatic L1Hs insertion rate in the Rett group, with 1.36 [range: 0.89–1.82] versus 1.22 [range:
298 0.63–1.66] per PFC neuron and 0.66 [range: 0.37–1.01] versus 0.54 [range: 0.34–0.72] per non-brain
299 cell (Fig 6C and S14 Table).
300
301 We next characterized the genome-wide germline L1Hs insertions. HAT-seq yielded greater than 320-
302 fold enrichment for KR, KNR, and UNK L1Hs insertions (S15 Table). On average, 814 KRs, 183
303 KNRs, and 10 UNKs were identified in each bulk sample (Table 2, S5–7 Table). Hierarchical clustering
304 based on L1Hs profiles correctly paired all neuronal samples with the non-neuronal tissue samples of
305 the same individual (Fig 6D). To experimentally validate the HAT-seq predicted germline insertions,
306 we performed 3' PCR validation on a random subset of polymorphic insertions from among the ten
307 individuals, including 8 sites out of 160 polymorphic KRs, 20 sites out of 451 KNRs, and 2 sites out
308 of 48 UNKs (S7 and S16 Table). As a result, all of the assayed sites were detected in 3' PCR, with
309 98.4% (120/122) and 100% (168/168) sensitivity and specificity, respectively (S16 Table and
310 Appendix 5). These results support that HAT-seq can reliably detect germline L1Hs insertions with
311 high sensitivity and specificity.
312

313 Previous studies have shown that intronic germline L1Hs insertions are sense-depleted (Ewing and
314 Kazazian, 2010; Smit, 1999; Upton et al., 2015). As expected, the germline insertions identified in this
315 study were significantly sense-depleted to the transcripts (633/1,544 [41%], $p = 1.6\times10^{-12}$, binomial
316 test; Fig 6E and S13 Table). It is important to ask the question: whether such orientation bias for
317 germline insertions is resulted from natural selection or insertional preference? To address this, we
318 chose somatic L1Hs insertions as internal reference to control confounding factors. We compared the
319 orientation bias between germline and somatic L1Hs insertions in transcripts and found that germline
320 insertions were significantly sense-depleted than somatic insertions (odds ratio [OR] = 0.79, p =
321 7.9×10^{-4}, Fisher's exact test; Fig 6E and S13 Table). Because somatic L1Hs insertions only affected a
322 small proportion of cells and thus they should undergo weaker selective pressure than germline
323 insertions, our results suggested that natural selection may play a major role in shaping the sense-
324 depleted distribution of germline L1Hs insertions.
325

326 **Discussion**

327 Here, we present HAT-seq, a bulk DNA sequencing method to profile genome-wide L1Hs insertions
328 from physiologically normal and pathological human tissues. We demonstrated that, in addition to
329 neuronal cells (Erwin et al., 2016; Evrony et al., 2012; Evrony et al., 2015; Macia et al., 2017; Upton
330 et al., 2015), L1Hs also retrotransposed in a variety of non-brain tissues and cell types during normal
331 development and contributed to the inter-cellular diversity of the human genome. Using high-
332 throughput sequencing-based quantitative analysis, we found that somatic insertions occurred at a
333 higher rate in brain than in non-brain tissues, consistent with previous studies (Coufal et al., 2009).

334 Previous qPCR and single-cell genomic studies have resulted in conflicting estimates of the frequency
335 of somatic insertions in neurons: ~80 L1 insertions per neuron (Coufal et al., 2009), < 0.04–0.6 L1
336 insertions per neuron (Evrony et al., 2012), 13.7 L1 insertions per neuron (Upton et al., 2015), or
337 ~0.58–1 somatic L1-associated variants per neuron (Erwin et al., 2016). Differential estimates might
338 result from differences in WGA and signal enrichment methods. Using a bulk DNA sequencing
339 approach, we estimated the rate of somatic insertions to be 0.63–1.66 L1Hs insertions per PFC neuron
340 in healthy individuals (Fig 6B and S14 Table).
341
342 Clonally distributed insertions are prevalent in normal brain (Evrony et al., 2015). Increasing evidence
343 suggests that neuronal L1s retrotransposition contributes to the susceptibility to and pathophysiology
344 of neurological disorders, including Rett syndrome (Muotri et al., 2010), schizophrenia (Bundo et al.,
345 2014) and Alzheimer's disease (Guo et al., 2018). We observed that, in PFC neurons of Rett patients,
346 clonal somatic insertions were enriched in introns, and these clonal intronic insertions were
347 significantly enriched in the sense orientation (Fig 5C–D). In particular, in Rett patient UMB#4516,
348 we found a full-length, sense-orientated, intronic somatic insertion (chr20:2392172) in *TGM6* (S6A-D
349 Fig and S11 Table), a gene associated with central nervous system development and motor function
350 (Thomas et al., 2013), which could potentially dysregulate gene expression (Han et al., 2004). We
351 found that 6.34% of fibroblasts and 2.87% of PFC neurons contained this L1Hs insertion (S8A–F Fig
352 and S10 Table), suggesting that this insertion might occurring in the 16-cell or 32-cell stages during
353 morula stage. Mutations in *TGM6* are associated with spinocerebellar ataxia type 35, one of a group
354 of genetic disorders characterized by poor coordination of hands, gait, speech, and eye movements as
355 well as frequent atrophy of the cerebellum (Guo et al., 2014; Li et al., 2013; Wang et al., 2010).

356 According to the clinical records, UMB#4516 had slight cerebral atrophy and cerebellar degeneration,
357 could not hold things in her hands, and her speech development ceased at 16 months of age; these
358 phenotypes were absent in the other four patients with Rett syndrome. Taken together, our data
359 indicated that this clonal L1Hs insertion of *TGM6* might be correlated with the distinct clinical
360 phenotype of UMB#4516.
361
362 Previous studies have provided evidence for significant selection against older L1 elements that are
363 non-polymorphic (Boissinot et al., 2001; Ewing and Kazazian, 2010). To characterize the insertion
364 pattern of L1 with minimal influence from selective pressure, experimental methods were developed
365 for recovery of novel L1 insertions in cultured cells (Gilbert et al., 2005; Symer et al., 2002). Using
366 HAT-seq method, we were able to distinguish somatic L1Hs insertions from germline L1Hs insertions
367 within the same individual. To determine whether the sense-depleted germline insertion was resulted
368 from natural selection or insertional preference, we used somatic insertion as internal reference to
369 control confounding factors such as intrinsic insertion preference and compared germline with somatic
370 insertions. Our results suggested that natural selection shaped a sense-depleted distribution of germline
371 L1Hs insertions in the human genome.
372
373 Several PCR-based bulk sequencing methods, such as ATLAS (Badge et al., 2003), L1-seq (Ewing
374 and Kazazian, 2010), TIP-seq (Tang et al., 2017), bulk SLAV-seq (Erwin et al., 2016), and ATLAS-seq
375 (Philippe and Cristofari, 2016), have been developed to identify germline L1Hs insertions.
376 Furthermore, L1-seq and TIP-seq have been successfully used in the identification of somatic
377 insertions in tumors (Achanta et al., 2016; Doucet-O'Hare et al., 2015; Ewing et al., 2015; Solyom et

al., 2012; Tang et al., 2017). Due to clonal expansion during tumorigenesis, such insertions could affect numerous cells in tumors. To our knowledge, HAT-seq is the first PCR-based bulk sequencing method to identify rare somatic insertions in a subset of cells—even unique cells—in non-tumor tissues. HAT-seq provides not only the genomic positions of somatic insertions but also the allele fraction of each insertion, which is informative for inferring the timing when the insertion has occurred. The sensitivities of HAT-seq for low-frequency somatic L1Hs insertions were relatively low (~30% for insertions present in < 1% fraction of cells). One possible explanation was that some signals of insertion were lost during library construction and NGS sequencing, e.g. sonic fragmentation, clean-ups, size selection, and loading library to sequencer. Single-cell whole genome and targeted sequencing approaches have been used to identify both TPRT-mediated and endonuclease-independent insertions (Erwin et al., 2016; Evrony et al., 2012; Evrony et al., 2015; Upton et al., 2015), where the signal of somatic insertions can be as high as germline heterozygous insertions in single-cell level. However, such single-cell approaches cannot achieve increased sensitivity without cost (Evrony et al., 2016). For example, to detect a given insertion with 0.1% mosaicism, more than 1,000 single cells may need to be amplified and sequenced. Therefore, compared with single-cell approaches, HAT-seq was eligible to identify a large number of somatic L1Hs insertions in a more cost-effective way.

Based on our experimental design, assembling overlapped read pairs into contigs can provide sequence information fully spanning the L1Hs integration sites, enabling downstream false-positive filtering based on both sequence features and read-count. However, a portion of read pairs were unable to be merged into contigs because the inaccurate size-selection during library construction. Applying the same filtering strategy, we re-analyzed these unassembled read pairs and revealed 11 clonal insertion

candidates. Further PCR experiments only validate one of these candidates (9%, S10 Table). Because the key filter "chimera within poly-A tail" was not applicable for unassembled read pairs, our sequence analysis suggested that chimeric molecules bridging within the poly-A tail was the major source of false-positives for unassembled data (see details in Materials and Methods). As shown in the statistics of positive control libraries (S2 Table) and experimental validation, the unassembled data could provide additional signals of somatic L1Hs insertions but require careful analysis and rigorous validation to address technical artifacts. Further gains in statistical power will be benefited from increased sample size and improved efficiency of HAT-seq.

Several unresolved technical challenges might constrain the total number of detectable L1Hs insertions by the current version of HAT-seq, including the identification of insertions in repetitive regions with low mappability (such as pre-existing L1 germline insertions) and 3' truncated insertions. With rapid innovations in sequencing technology, higher throughput and longer read length will markedly improve the performance of HAT-seq. Future studies that profile all active retrotransposons (i.e., L1Hs, Alu, and SVA) in a variety of cell types, tissues, and developmental stages will shed new light on the dynamics of somatic retrotransposition under host regulation and help to uncover their roles in human disease.

Acknowledgements

We acknowledge the UMB Brain and Tissue Bank (University of Maryland, Baltimore, MD) and the Lieber Institute for Brain Development (Baltimore, MD) for providing postmortem human tissues. We

are grateful to Drs Eunjung Alice Lee, Daniel R. Weinberger, Li-Lin Du, Meng-Qiu Dong, Yu Zhang, Ge Gao, Louis Tao, Cheng Li, Jian Lu, and Manyuan Long for their insightful comments and suggestions. We thank Drs Kazuya Iwamoto and Miki Bundo for providing detailed protocols of nuclei isolation. We thank Dr. Timothy W. Yu for providing experimental resources in the revision. We thank the reviewers for constructive feedback on the manuscript.

Author contributions

Adam Yongxin Ye

Formal analysis, Methodology, Visualization, Writing-original draft

August Yue Huang

Conceptualization, Resources, Supervision, Writing—review and editing

Boxun Zhao

Conceptualization, Data curation, Formal analysis, Investigation, Methodology, Project administration, Validation, Visualization, Writing—original draft, Writing—review and editing

Jing Guo

Data curation, Methodology, Validation

Liping Wei

Conceptualization, Funding acquisition, Resources, Supervision, Writing—review and editing

Linlin Yan

Formal analysis

Thomas M. Hyde

Resources

Qing-Rong Liu

Methodology

Qixi Wu

Conceptualization, Investigation, Methodology, Writing—review and editing

Xianing Zheng

Methodology

Xiaoxu Yang

Validation, Visualization

Competing interests

No conflicts of interest.

465 **References**

466 Achanta, P., Steranka, J.P., Tang, Z., Rodic, N., Sharma, R., Yang, W.R., Ma, S., Grivainis, M., Huang,
467 C.R.L., Schneider, A.M., *et al.* (2016). Somatic retrotransposition is infrequent in glioblastomas. Mob
468 DNA *7*, 22.

469 Amir, R.E., Van den Veyver, I.B., Wan, M., Tran, C.Q., Francke, U., and Zoghbi, H.Y. (1999). Rett
470 syndrome is caused by mutations in X-linked MECP2, encoding methyl-CpG-binding protein 2. Nat
471 Genet *23*, 185-188.

472 Badge, R.M., Alisch, R.S., and Moran, J.V. (2003). ATLAS: a system to selectively identify human-
473 specific L1 insertions. Am J Hum Genet *72*, 823-838.

474 Bao, W., Kojima, K.K., and Kohany, O. (2015). Repbase Update, a database of repetitive elements in
475 eukaryotic genomes. Mob DNA *6*, 11.

476 Boissinot, S., Entezam, A., and Furano, A.V. (2001). Selection against deleterious LINE-1-containing
477 loci in the human lineage. Mol Biol Evol *18*, 926-935.

478 Bundo, M., Toyoshima, M., Okada, Y., Akamatsu, W., Ueda, J., Nemoto-Miyauchi, T., Sunaga, F.,
479 Toritsuka, M., Ikawa, D., Kakita, A., *et al.* (2014). Increased l1 retrotransposition in the neuronal
480 genome in schizophrenia. Neuron *81*, 306-313.

481 Campbell, I.M., Shaw, C.A., Stankiewicz, P., and Lupski, J.R. (2015). Somatic mosaicism:
482 implications for disease and transmission genetics. Trends Genet *31*, 382-392.

483 Cost, G.J., Feng, Q., Jacquier, A., and Boeke, J.D. (2002). Human L1 element target-primed reverse
484 transcription in vitro. EMBO J *21*, 5899-5910.

485 Coufal, N.G., Garcia-Perez, J.L., Peng, G.E., Yeo, G.W., Mu, Y., Lovci, M.T., Morell, M., O'Shea, K.S.,
486 Moran, J.V., and Gage, F.H. (2009). L1 retrotransposition in human neural progenitor cells. Nature

487 *460*, 1127-1131.

488 Doucet-O'Hare, T.T., Rodic, N., Sharma, R., Darbari, I., Abril, G., Choi, J.A., Young Ahn, J., Cheng,
489 Y., Anders, R.A., Burns, K.H., *et al.* (2015). LINE-1 expression and retrotransposition in Barrett's
490 esophagus and esophageal carcinoma. Proc Natl Acad Sci U S A *112*, E4894-4900.

491 Erwin, J.A., Marchetto, M.C., and Gage, F.H. (2014). Mobile DNA elements in the generation of
492 diversity and complexity in the brain. Nat Rev Neurosci *15*, 497-506.

493 Erwin, J.A., Paquola, A.C., Singer, T., Gallina, I., Novotny, M., Quayle, C., Bedrosian, T.A., Alves,
494 F.I., Butcher, C.R., Herdy, J.R., *et al.* (2016). L1-associated genomic regions are deleted in somatic
495 cells of the healthy human brain. Nat Neurosci *19*, 1583-1591.

496 Evrony, G.D., Cai, X., Lee, E., Hills, L.B., Elhosary, P.C., Lehmann, H.S., Parker, J.J., Atabay, K.D.,
497 Gilmore, E.C., Poduri, A., *et al.* (2012). Single-neuron sequencing analysis of L1 retrotransposition
498 and somatic mutation in the human brain. Cell *151*, 483-496.

499 Evrony, G.D., Lee, E., Mehta, B.K., Benjamini, Y., Johnson, R.M., Cai, X., Yang, L., Haseley, P.,
500 Lehmann, H.S., Park, P.J., *et al.* (2015). Cell lineage analysis in human brain using endogenous
501 retroelements. Neuron *85*, 49-59.

502 Evrony, G.D., Lee, E., Park, P.J., and Walsh, C.A. (2016). Resolving rates of mutation in the brain
503 using single-neuron genomics. Elife *5*.

504 Ewing, A.D., Gacita, A., Wood, L.D., Ma, F., Xing, D., Kim, M.S., Manda, S.S., Abril, G., Pereira, G.,
505 Makohon-Moore, A., *et al.* (2015). Widespread somatic L1 retrotransposition occurs early during
506 gastrointestinal cancer evolution. Genome Res *25*, 1536-1545.

507 Ewing, A.D., and Kazazian, H.H., Jr. (2010). High-throughput sequencing reveals extensive variation
508 in human-specific L1 content in individual human genomes. Genome Res *20*, 1262-1270.

509 Faulkner, G.J., and Billon, V. (2018). L1 retrotransposition in the soma: a field jumping ahead. Mobile
510 DNA *9*, 22.
511 Faulkner, G.J., and Garcia-Perez, J.L. (2017). L1 Mosaicism in Mammals: Extent, Effects, and
512 Evolution. Trends Genet *33*, 802-816.
513 Frank, S.A. (2010). Evolution in health and medicine Sackler colloquium: Somatic evolutionary
514 genomics: mutations during development cause highly variable genetic mosaicism with risk of cancer
515 and neurodegeneration. Proc Natl Acad Sci U S A *107 Suppl 1*, 1725-1730.
516 Gabel, H.W., Kinde, B., Stroud, H., Gilbert, C.S., Harmin, D.A., Kastan, N.R., Hemberg, M., Ebert,
517 D.H., and Greenberg, M.E. (2015). Disruption of DNA-methylation-dependent long gene repression
518 in Rett syndrome. Nature *522*, 89-93.
519 Gilbert, N., Lutz, S., Morrish, T.A., and Moran, J.V. (2005). Multiple fates of L1 retrotransposition
520 intermediates in cultured human cells. Mol Cell Biol *25*, 7780-7795.
521 Goodier, J.L. (2014). Retrotransposition in tumors and brains. Mob DNA *5*, 11.
522 Grandi, F.C., Rosser, J.M., and An, W. (2013). LINE-1-derived poly(A) microsatellites undergo rapid
523 shortening and create somatic and germline mosaicism in mice. Mol Biol Evol *30*, 503-512.
524 Grun, D., and van Oudenaarden, A. (2015). Design and Analysis of Single-Cell Sequencing
525 Experiments. Cell *163*, 799-810.
526 Guo, C., Jeong, H.-H., Hsieh, Y.-C., Klein, H.-U., Bennett, D.A., Jager, P.L., Liu, Z., and Shulman,
527 J.M. (2018). Tau Activates Transposable Elements in Alzheimer's Disease. Cell reports *23*, 2874-2880.
528 Guo, Y.C., Lin, J.J., Liao, Y.C., Tsai, P.C., Lee, Y.C., and Soong, B.W. (2014). Spinocerebellar ataxia
529 35: novel mutations in TGM6 with clinical and genetic characterization. Neurology *83*, 1554-1561.
530 Han, J.S., Szak, S.T., and Boeke, J.D. (2004). Transcriptional disruption by the L1 retrotransposon and

531 implications for mammalian transcriptomes. Nature *429*, 268-274.

532 Hancks, D.C., and Kazazian, H.H., Jr. (2012). Active human retrotransposons: variation and disease.
533 Curr Opin Genet Dev *22*, 191-203.

534 Jurka, J. (1997). Sequence patterns indicate an enzymatic involvement in integration of mammalian
535 retroposons. Proc Natl Acad Sci U S A *94*, 1872-1877.

536 Kazazian, H.H., Jr., and Moran, J.V. (2017). Mobile DNA in Health and Disease. N Engl J Med *377*,
537 361-370.

538 King, I.F., Yandava, C.N., Mabb, A.M., Hsiao, J.S., Huang, H.S., Pearson, B.L., Calabrese, J.M.,
539 Starmer, J., Parker, J.S., Magnuson, T.*, et al.* (2013). Topoisomerases facilitate transcription of long
540 genes linked to autism. Nature *501*, 58-62.

541 Li, M., Pang, S.Y., Song, Y., Kung, M.H., Ho, S.L., and Sham, P.C. (2013). Whole exome sequencing
542 identifies a novel mutation in the transglutaminase 6 gene for spinocerebellar ataxia in a Chinese family.
543 Clin Genet *83*, 269-273.

544 Luan, D.D., Korman, M.H., Jakubczak, J.L., and Eickbush, T.H. (1993). Reverse transcription of
545 R2Bm RNA is primed by a nick at the chromosomal target site: a mechanism for non-LTR
546 retrotransposition. Cell *72*, 595-605.

547 Macia, A., Widmann, T.J., Heras, S.R., Ayllon, V., Sanchez, L., Benkaddour-Boumzaouad, M., Munoz-
548 Lopez, M., Rubio, A., Amador-Cubero, S., Blanco-Jimenez, E.*, et al.* (2017). Engineered LINE-1
549 retrotransposition in nondividing human neurons. Genome Res *27*, 335-348.

550 Mir, A.A., Philippe, C., and Cristofari, G. (2015). euL1db: the European database of L1HS
551 retrotransposon insertions in humans. Nucleic Acids Res *43*, D43-47.

552 Morrish, T.A., Gilbert, N., Myers, J.S., Vincent, B.J., Stamato, T.D., Taccioli, G.E., Batzer, M.A., and

553 Moran, J.V. (2002). DNA repair mediated by endonuclease-independent LINE-1 retrotransposition.
554 Nat Genet *31*, 159-165.
555 Mullen, R.J., Buck, C.R., and Smith, A.M. (1992). NeuN, a neuronal specific nuclear protein in
556 vertebrates. Development *116*, 201-211.
557 Muotri, A.R., Marchetto, M.C., Coufal, N.G., Oefner, R., Yeo, G., Nakashima, K., and Gage, F.H.
558 (2010). L1 retrotransposition in neurons is modulated by MeCP2. Nature *468*, 443-446.
559 Navin, N.E. (2015). The first five years of single-cell cancer genomics and beyond. Genome Res *25*,
560 1499-1507.
561 Ovchinnikov, I., Troxel, A.B., and Swergold, G.D. (2001). Genomic characterization of recent human
562 LINE-1 insertions: evidence supporting random insertion. Genome Res *11*, 2050-2058.
563 Philippe, C., and Cristofari, G. (2016). Activation of individual L1 retrotransposon instances is
564 restricted to cell-type dependent permissive loci. eLife.
565 Poduri, A., Evrony, G.D., Cai, X., and Walsh, C.A. (2013). Somatic mutation, genomic variation, and
566 neurological disease. Science *341*, 1237758.
567 Reilly, M.T., Faulkner, G.J., Dubnau, J., Ponomarev, I., and Gage, F.H. (2013). The role of transposable
568 elements in health and diseases of the central nervous system. J Neurosci *33*, 17577-17586.
569 Skene, P.J., Illingworth, R.S., Webb, S., Kerr, A.R., James, K.D., Turner, D.J., Andrews, R., and Bird,
570 A.P. (2010). Neuronal MeCP2 is expressed at near histone-octamer levels and globally alters the
571 chromatin state. Mol Cell *37*, 457-468.
572 Smit, A.F. (1999). Interspersed repeats and other mementos of transposable elements in mammalian
573 genomes. Curr Opin Genet Dev *9*, 657-663.
574 Solyom, S., Ewing, A.D., Rahrmann, E.P., Doucet, T., Nelson, H.H., Burns, M.B., Harris, R.S., Sigmon,

575 D.F., Casella, A., Erlanger, B., *et al.* (2012). Extensive somatic L1 retrotransposition in colorectal
576 tumors. Genome Res *22*, 2328-2338.
577 Symer, D.E., Connelly, C., Szak, S.T., Caputo, E.M., Cost, G.J., Parmigiani, G., and Boeke, J.D. (2002).
578 Human l1 retrotransposition is associated with genetic instability in vivo. Cell *110*, 327-338.
579 Tang, Z., Steranka, J.P., Ma, S., Grivainis, M., Rodic, N., Huang, C.R., Shih, I.M., Wang, T.L., Boeke,
580 J.D., Fenyo, D., *et al.* (2017). Human transposon insertion profiling: Analysis, visualization and
581 identification of somatic LINE-1 insertions in ovarian cancer. Proc Natl Acad Sci U S A *114*, E733-
582 E740.
583 Thomas, H., Beck, K., Adamczyk, M., Aeschlimann, P., Langley, M., Oita, R.C., Thiebach, L., Hils,
584 M., and Aeschlimann, D. (2013). Transglutaminase 6: a protein associated with central nervous system
585 development and motor function. Amino Acids *44*, 161-177.
586 Upton, K.R., Gerhardt, D.J., Jesuadian, J.S., Richardson, S.R., Sanchez-Luque, F.J., Bodea, G.O.,
587 Ewing, A.D., Salvador-Palomeque, C., van der Knaap, M.S., Brennan, P.M., *et al.* (2015). Ubiquitous
588 L1 mosaicism in hippocampal neurons. Cell *161*, 228-239.
589 Wang, J.L., Yang, X., Xia, K., Hu, Z.M., Weng, L., Jin, X., Jiang, H., Zhang, P., Shen, L., Guo, J.F., *et*
590 *al.* (2010). TGM6 identified as a novel causative gene of spinocerebellar ataxias using exome
591 sequencing. Brain *133*, 3510-3518.
592 Yu, F., Zingler, N., Schumann, G.G., and Stratling, W.H. (2001). Mecp2 represses L1 expression and
593 retrotransposition but not Alu transcription. Nucleic Acids Res *29*, 4493-4501.

594

595 **Figures**

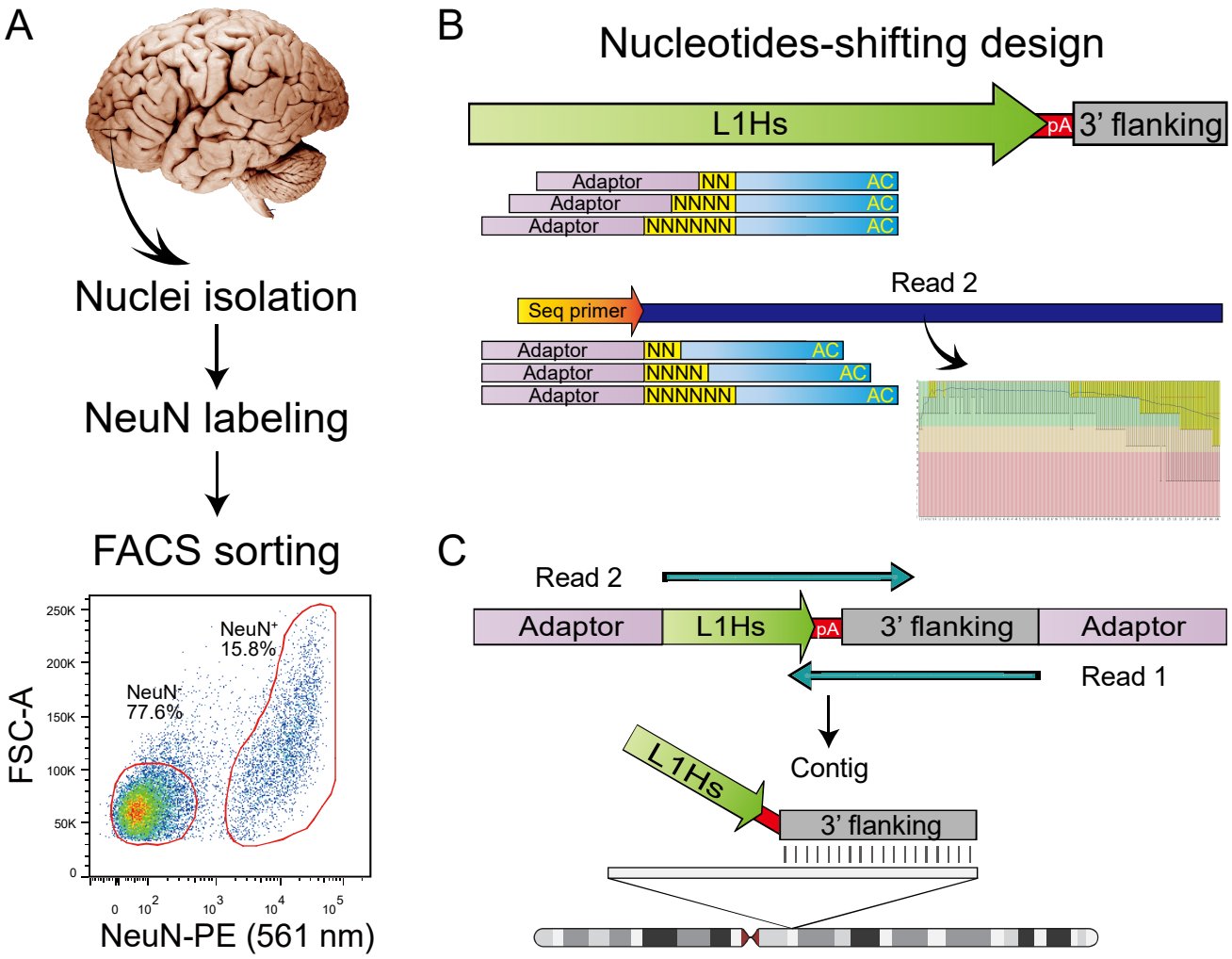

596
597

598 **Fig 1. Overview of human active transposon sequencing (HAT-seq).**

599 (A) Fluorescence-activated cell sorting (FACS) of prefrontal cortex (PFC) nuclei labeled with NeuN.

600 Two populations ($NeuN^+$ and $NeuN^-$) were sorted. (B) Schematic of the nucleotides-shifting design of

601 the HAT-seq method. By adding two, four, or six random nucleotides upstream of L1Hs-specific primer

602 (L1Hs-AC-28), we transformed the library from a uniform phase-0 amplicon library to a mixed library

603 with phase-2, phase-4, and phase-6 amplicons, which remarkedly improved the base calling accuracy

604 in Read 2. (C) HAT-seq libraries were sequenced with paired-end 150-bp reads. After merging paired

605 reads into contigs that fully spanned the L1Hs-genome 3' junction, genomic locations of each L1Hs

606 insertion were determined by the alignments of their 3' flanking genomic sequences.

607

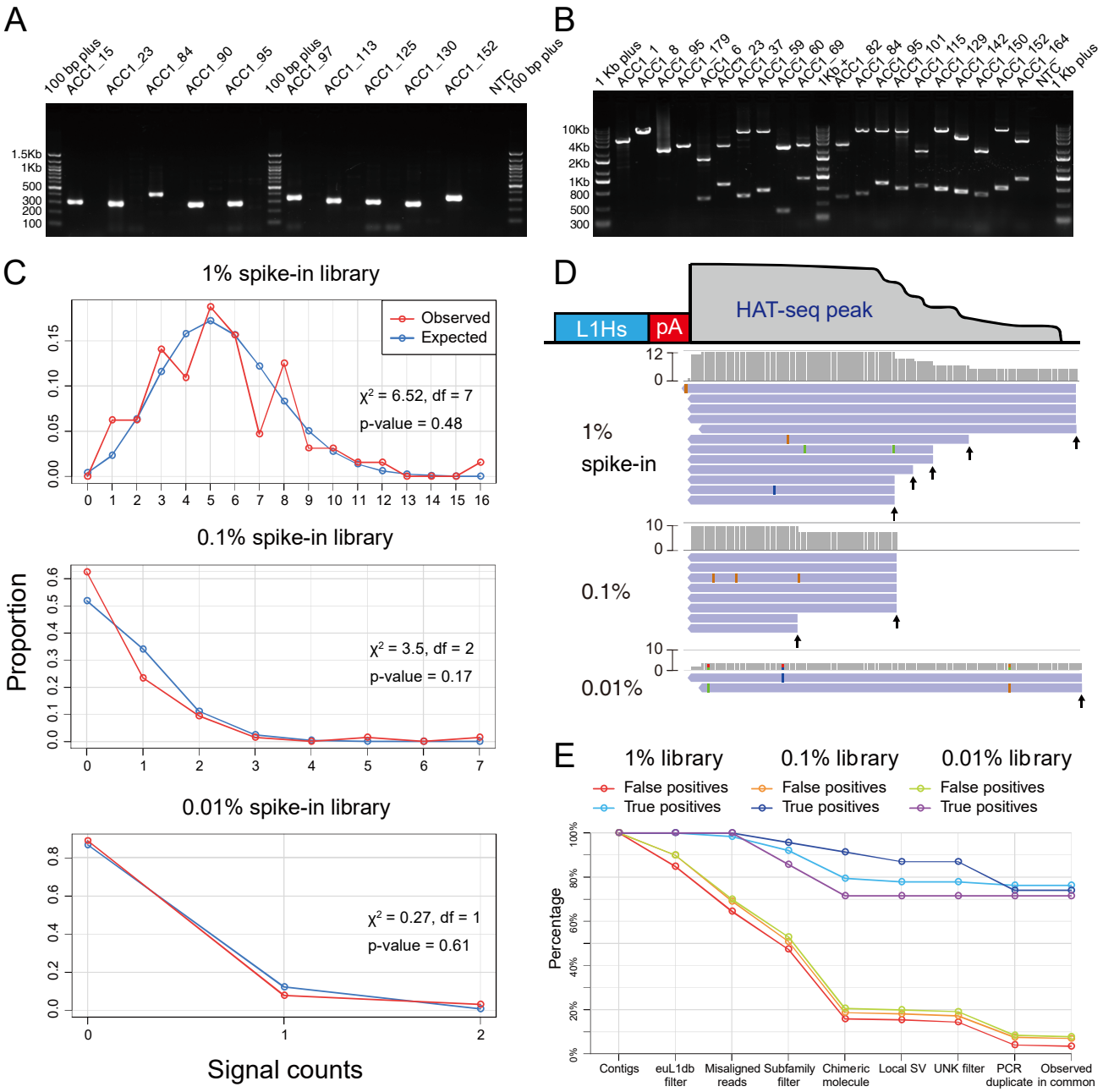
A
100 bp plus
ACC1_15
ACC1_23
ACC1_84
ACC1_90
ACC1_95
100 bp plus
ACC1_97
ACC1_113
ACC1_125
ACC1_130
ACC1_152
NTC
100 bp plus
1.5Kb
1Kb
500
300
200
100
B
1 Kb plus
ACC1_1
ACC1_8
ACC1_95
ACC1_179
ACC1_6
ACC1_23
ACC1_37
ACC1_59
ACC1_60
ACC1_69
1Kb+
ACC1_82
ACC1_84
ACC1_95
ACC1_101
ACC1_115
ACC1_129
ACC1_142
ACC1_150
ACC1_152
ACC1_164
NTC
1 Kb plus
10Kb
4Kb
2Kb
1Kb
800
500
300
C
1% spike-in library
Observed
Expected
χ² = 6.52, df = 7
p-value = 0.48
0.1% spike-in library
χ² = 3.5, df = 2
p-value = 0.17
0.01% spike-in library
χ² = 0.27, df = 1
p-value = 0.61
Proportion
Signal counts
D
L1Hs
pA
HAT-seq peak
1%
spike-in
0.1%
0.01%
E
1% library
0.1% library
0.01% library
False positives
True positives
Percentage
Contigs
euL1db filter
Misaligned reads
Subfamily filter
Chimeric molecule
Local SV
UNK filter
PCR duplicate
Observed in common

608
609

610 **Fig 2. HAT-seq performance evaluation using a positive control.**

611 (A) Representative gel image used for the identification of ACC1-specific insertions based on 3' PCR
612 analysis. For each site, genomic DNA from ACC1 and ACC2 was amplified using the same protocol.
613 NTC: negative control. (B) Representative gel image used for the zygosity analysis of ACC1-specific
614 insertions based on full-length PCR. The four sites on the left were homozygous L1Hs insertions and
615 the others were heterozygous L1Hs insertions. (C) The distributions of signal counts (reads with unique
616 start positions) per ACC1-specific insertion closely followed Poisson distributions (chi-squared
617 goodness-of-fit tests). (D) Representative ACC1-specific insertion (ACC1_132 at chr21:29069173) in
618 1%, 0.1%, and 0.01% spike-in libraries. Read coverage and supporting signal counts (unique start
619 positions were indicated by black arrows) were positively correlated with the spike-in concentration.
620 (E) The effectiveness of error filters. 64 ACC1-specific germline insertions in 1%, 0.1%, and 0.01%
621 spike-in libraries were considered as "true positives"; all other signals were considered as "false
622 positives", which might include both background noise and some true somatic insertions present in the
623 blood gDNA.
624

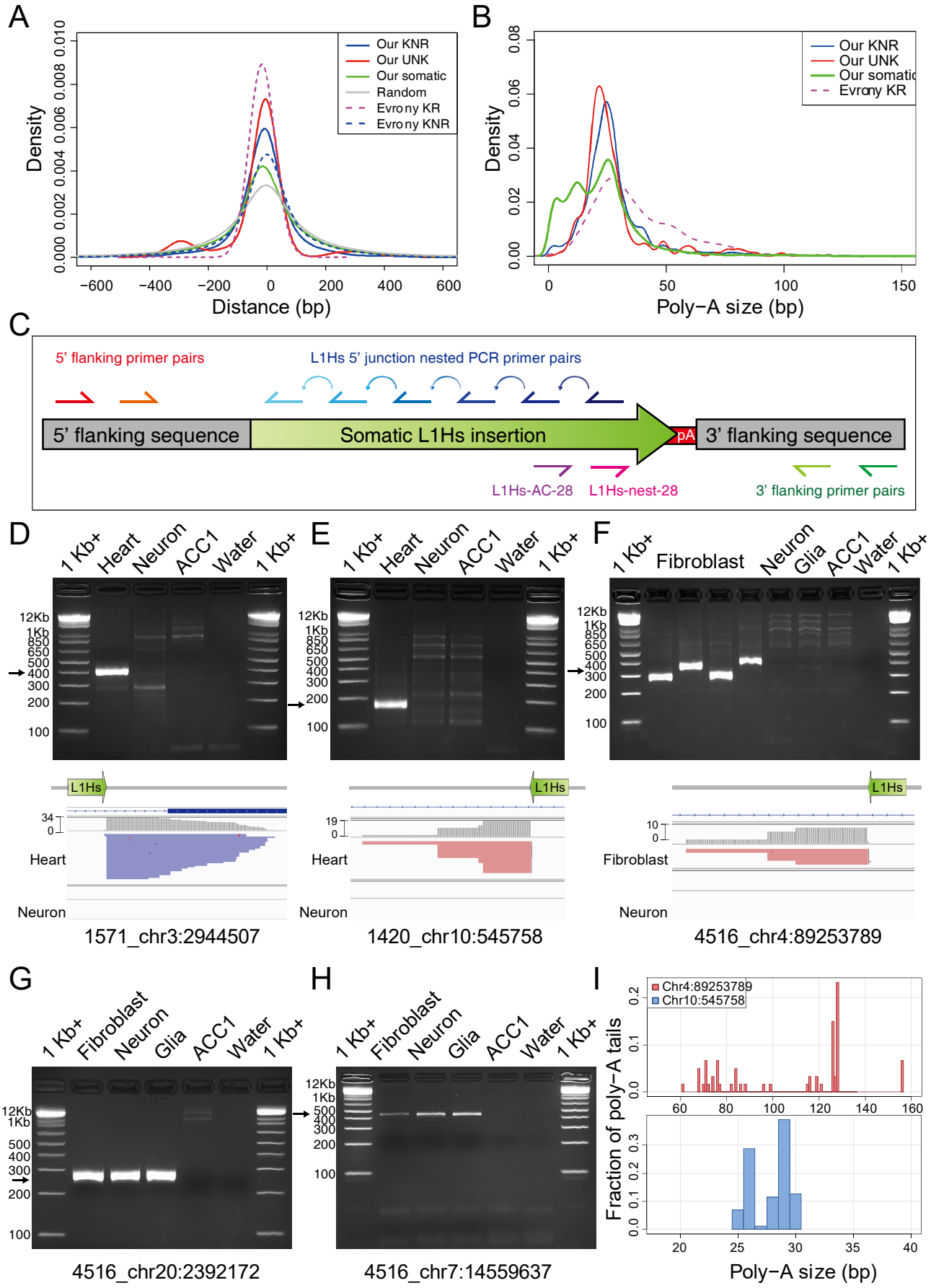
A
Density
Distance (bp)
Our KNR
Our UNK
Our somatic
Random
Evrony KR
Evrony KNR
B
Density
Poly−A size (bp)
Our KNR
Our UNK
Our somatic
Evrony KR
C
5' flanking primer pairs
L1Hs 5' junction nested PCR primer pairs
5' flanking sequence
Somatic L1Hs insertion
pA
3' flanking sequence
L1Hs-AC-28
L1Hs-nest-28
3' flanking primer pairs
D
1 Kb+
Heart
Neuron
ACC1
Water
1 Kb+
12Kb
1Kb
850
650
500
400
300
200
100
L1Hs
Heart
Neuron
1571_chr3:2944507
E
1 Kb+
Heart
Neuron
ACC1
Water
1 Kb+
L1Hs
Heart
Neuron
1420_chr10:545758
F
1 Kb+
Fibroblast
Neuron
Glia
ACC1
Water
1 Kb+
L1Hs
Fibroblast
Neuron
4516_chr4:89253789
G
1 Kb+
Fibroblast
Neuron
Glia
ACC1
Water
1 Kb+
4516_chr20:2392172
H
1 Kb+
Fibroblast
Neuron
Glia
ACC1
Water
1 Kb+
4516_chr7:14559637
I
Chr4:89253789
Chr10:545758
Fraction of poly−A tails
Poly−A size (bp)

627 **Fig 3. Profiling of somatic L1Hs insertions in multiple human tissues.**

628 (A) The density distributions of L1 EN motifs around L1Hs integration sites. L1 EN motifs included
629 seven specific motifs (TTAAAA, TTAAGA, TTAGAA, TTGAAA, TTAAAG, CTAAAA, TCAAAA).
630 "Evrony KR" and "Evrony KNR" are germline L1Hs insertions identified in Evrony *et al.* 2012. (B)
631 The density distributions of poly-A tail length for each category of L1Hs insertion. (C) The PCR
632 validation scheme and locations of primers used. (D)–(H) Representative gel images of 3' nested PCR
633 validation for putative clonal somatic insertions. The Integrative Genomics Viewer screenshots for
634 (D)–(F) showed the coverage track (gray) and the alignment track (blue for read strand [-]; red for read
635 strand [+]) from HAT-seq data. Black arrows indicated bands with target size. 1Kb +: 1 Kb Plus DNA
636 ladder. (I) Polymorphic poly-A tail sizes of clonal somatic insertions. Top: fibroblast-specific somatic
637 L1Hs insertion at chr4:89253789 from Rett patient UMB#4516. Bottom: heart-specific somatic L1Hs
638 insertion at chr10:545758 from Rett patient UMB#1420.
639

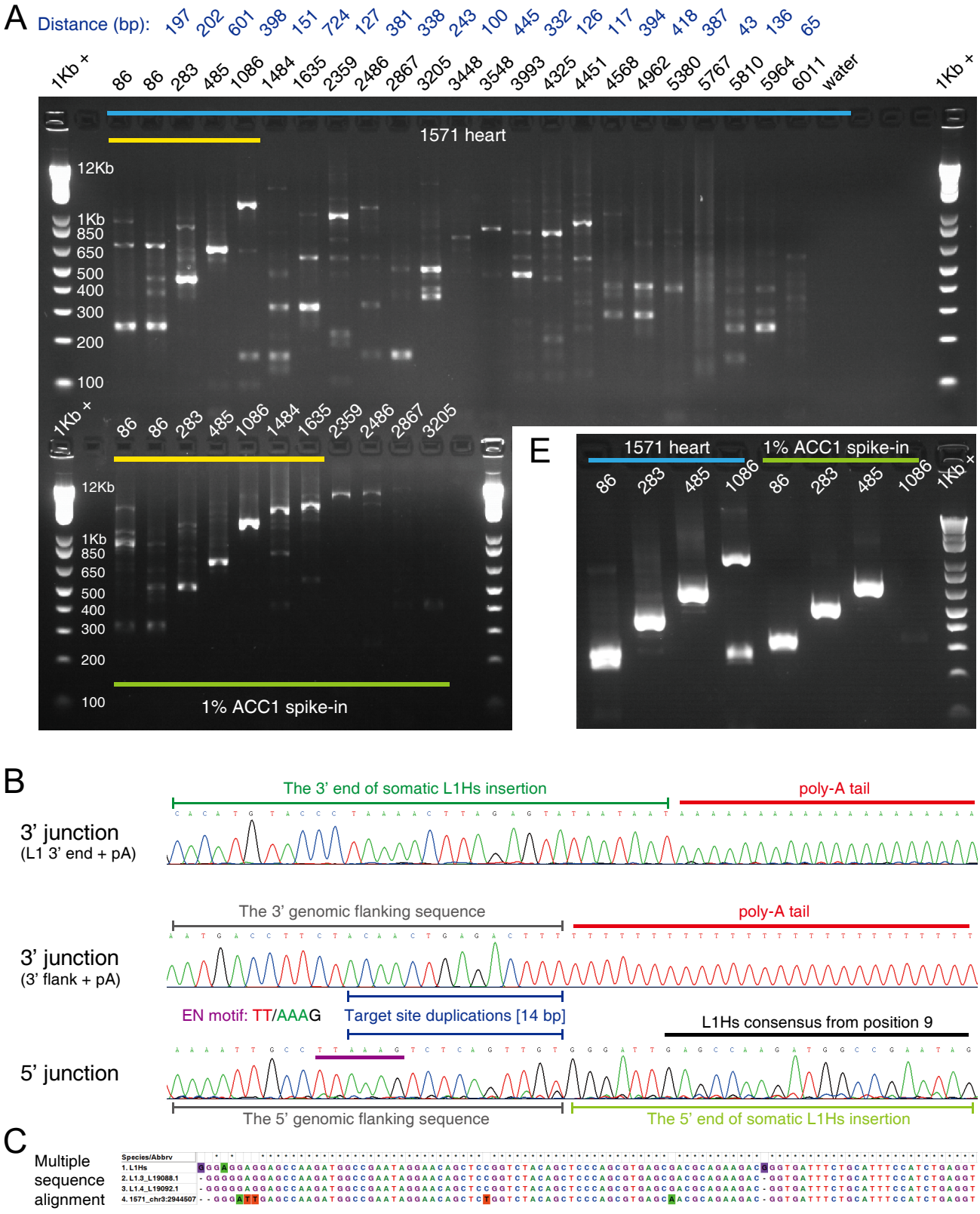
A
Distance (bp): 197 202 601 398 151 724 127 381 338 243 100 445 332 126 117 394 418 387 43 136 65
1Kb + 86 86 283 485 1086 1484 1635 2359 2486 2867 3205 3448 3548 3993 4325 4451 4568 4962 5380 5767 5810 5964 6011 water 1Kb +
1571 heart
12Kb
1Kb
850
650
500
400
300
200
100
1Kb + 86 86 283 485 1086 1484 1635 2359 2486 2867 3205
12Kb
1Kb
850
650
500
400
300
200
100
1% ACC1 spike-in
E
1571 heart
1% ACC1 spike-in
86 283 485 1086 86 283 485 1086 1Kb +
B
The 3' end of somatic L1Hs insertion
poly-A tail
3' junction
(L1 3' end + pA)
The 3' genomic flanking sequence
poly-A tail
3' junction
(3' flank + pA)
EN motif: TT/AAAG
Target site duplications [14 bp]
L1Hs consensus from position 9
5' junction
The 5' genomic flanking sequence
The 5' end of somatic L1Hs insertion
C
Multiple
sequence
alignment
Species/Abbrv
1. L1Hs
2. L1.3_L19088.1
3. L1.4_L19092.1
4. 1571_chr3:2944507
D
EN motif
TT/AAAG
A>50
14 bp
5' flanking sequence
TSD
somatic full-length L1Hs insertion
pA
TSD
3' flanking sequence

Fig 4. A full-length heart-specific L1Hs insertion in a healthy individual.

(A) The agarose gel image of 5' junction nested PCR validation for the heart-specific L1Hs insertion in the healthy individual (UMB#1571). The location of primers used in 5' junction PCR assays were labeled on the top of each lane. The distances between each primer pairs were labeled on the top (dark blue). The blue line indicated that the heart gDNA from UMB#1571 was used as template. The green line indicated the positive control assays where 1% ACC1 spike-in gDNA was used as template and the 5' junction of a heterozygous, full-length L1Hs insertion (ACC1_16) was amplified by 5' junction nested PCR assays (S11 Table and Appendix 4). The yellow line indicated stair-step bands with expected distance between each pair of 5' PCR reactions. 1Kb +: 1 Kb Plus DNA ladder. (B) The Sanger sequencing chromatograms of the 3' and 5' junctions of somatic insertion (1571_chr3:2944507). Top: the 3' junction of L1Hs insertion including the 3' end of L1Hs element and its poly-A tail. Middle: the poly-A tail and 3' flanking genomic sequence of L1Hs insertion. Bottom: the 5' junction of L1Hs insertion including the 5' end of L1Hs elements and its 5' flanking genomic sequence. The purple line indicated the sequence of the L1 EN motif. The blue lines indicated the sequence of TSDs. (C) The multiple sequence alignment. Sequence set included the 5' junction sequence of somatic L1Hs insertion (1571_chr3:2944507) and three L1Hs consensus sequences (L1Hs Repbase consensus and two hot L1s in human [L1.3 and L1.4]). (D) The schematic structure of the full-length heart-specific L1Hs insertion in the healthy individual (UMB#1571). (E) The agarose gel image of 5' junction PCR assays, in which the PCR products of filled-in site from the full-length PCR were used as templates. The location of primers used in 5' junction PCR assays were labeled on the top of each lane. The blue line indicated "full-length PCR + 5' junction PCR" assays in which the heart gDNA from UMB#1571 was used as template. The green line indicated the matched positive control assays where 1% ACC1

664 spike-in gDNA was used as template and the 5' junction of a heterozygous, full-length L1Hs insertion

665 (ACC1_16) was amplified by "full-length PCR + 5' junction PCR" assays.

666

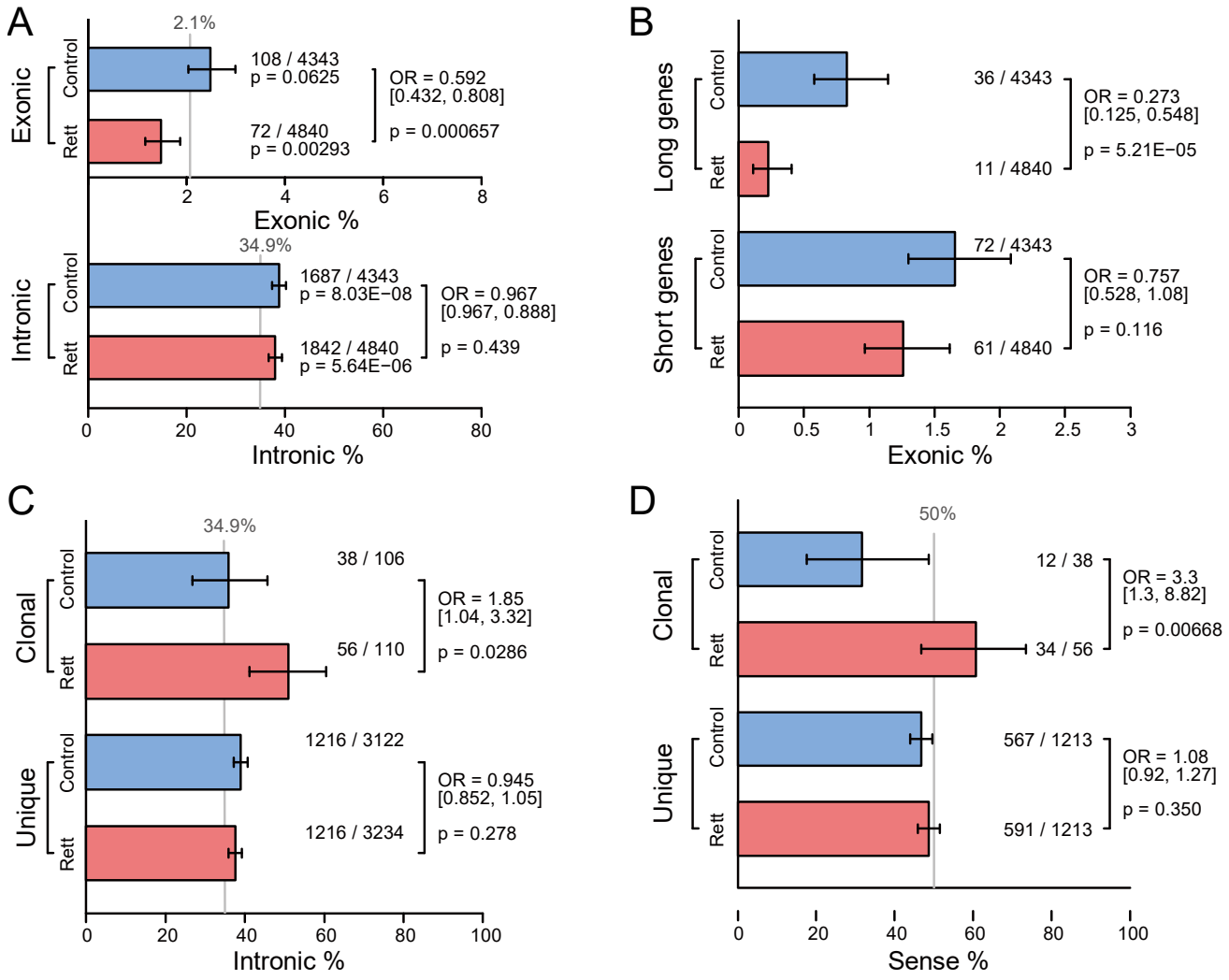
A
Exonic
Control
Rett
2.1%
108 / 4343
p = 0.0625
72 / 4840
p = 0.00293
OR = 0.592
[0.432, 0.808]
p = 0.000657
Exonic %
Intronic
34.9%
1687 / 4343
p = 8.03E−08
1842 / 4840
p = 5.64E−06
OR = 0.967
[0.967, 0.888]
p = 0.439
Intronic %
B
Long genes
36 / 4343
11 / 4840
OR = 0.273
[0.125, 0.548]
p = 5.21E−05
Short genes
72 / 4343
61 / 4840
OR = 0.757
[0.528, 1.08]
p = 0.116
Exonic %
C
Clonal
34.9%
38 / 106
56 / 110
OR = 1.85
[1.04, 3.32]
p = 0.0286
Unique
1216 / 3122
1216 / 3234
OR = 0.945
[0.852, 1.05]
p = 0.278
Intronic %
D
Clonal
50%
12 / 38
34 / 56
OR = 3.3
[1.3, 8.82]
p = 0.00668
Unique
567 / 1213
591 / 1213
OR = 1.08
[0.92, 1.27]
p = 0.350
Sense %

669 **Fig 5. Abnormal L1Hs mobilization in patients with Rett syndrome.**

670 (A) Percentages of somatic L1Hs insertions in exons and introns. (B) Percentages of somatic L1Hs
671 insertions in exons of long (> 100 kb) and short genes (< 100 kb). (C) Percentages of clonal and "unique"
672 somatic L1Hs insertions in introns. (D) Percentages of sense-oriented "unique" and clonal somatic
673 L1Hs insertions. The gray lines in (A) and (C) denoted the expected proportion determined by the
674 exact base-pair count of that specific region relative to the human genome. The gray line in (D)
675 represented the expected proportion if the insertions occurred randomly in both directions. Error bars
676 in (A)–(D) indicated the 95% confidence intervals. Among "unique" somatic L1Hs insertions, some
677 insertions might belong to clonal somatic insertion but supported with only one read due to random
678 sampling.
679

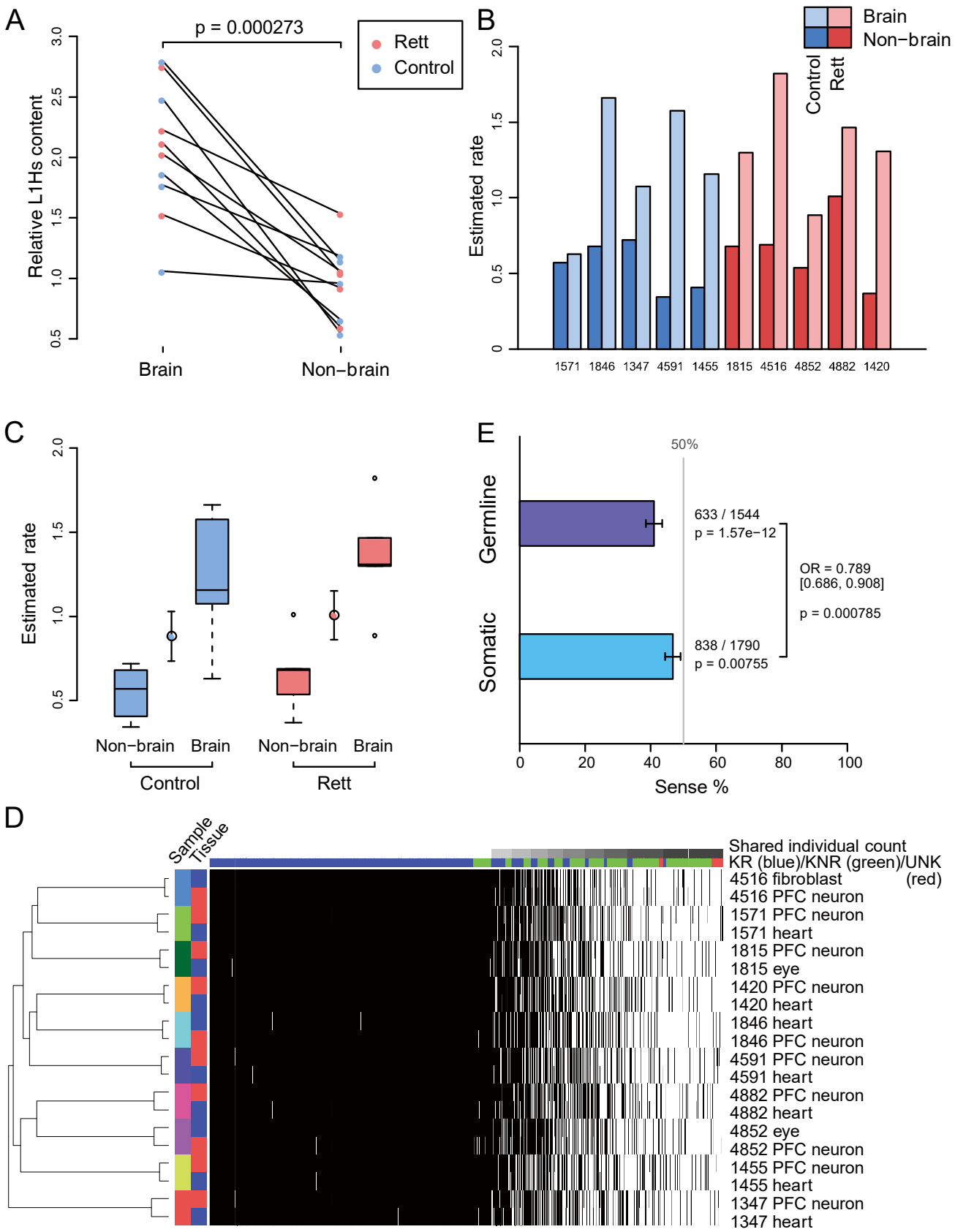
A
p = 0.000273
Rett
Control
Relative L1Hs content
Brain
Non−brain
B
Brain
Non−brain
Control
Rett
Estimated rate
1571 1846 1347 4591 1455 1815 4516 4852 4882 1420
C
Estimated rate
Non−brain Brain Non−brain Brain
Control
Rett
E
50%
Germline
Somatic
633 / 1544
p = 1.57e−12
OR = 0.789
[0.686, 0.908]
p = 0.000785
838 / 1790
p = 0.00755
Sense %
D
Sample
Tissue
Shared individual count
KR (blue)/KNR (green)/UNK (red)
4516 fibroblast
4516 PFC neuron
1571 PFC neuron
1571 heart
1815 PFC neuron
1815 eye
1420 PFC neuron
1420 heart
1846 heart
1846 PFC neuron
4591 PFC neuron
4591 heart
4882 PFC neuron
4882 heart
4852 eye
4852 PFC neuron
1455 PFC neuron
1455 heart
1347 PFC neuron
1347 heart

682 **Fig 6. Genome-wide patterns of somatic and germline L1Hs insertions.**

683 (A) Relative somatic L1Hs content in PFC neurons and non-brain tissue from the same donor. The
684 read count ratio of somatic insertions to germline KNR was calculated and then normalized relative
685 to the average value of non-brain samples. The linked dots represented pairs of brain and non-brain
686 samples obtained from the same individual. (B) Histogram of estimated rate of somatic L1Hs
687 insertions in each of tissue samples from the same donor based on the germline KNR copy number
688 of each individual. (C) Estimated rate of somatic L1Hs insertions for different tissue types and
689 cohorts. Error bars denoted the standard error of the mean (S.E.M). (D) Hierarchical clustering of all
690 samples sequenced in this study. Each row represented a sample, and each column represents an
691 L1Hs germline insertion. Black and white squares indicated the presence or absence of insertion,
692 respectively. Column annotations showed categories for known reference (KR; blue), known non-
693 reference (KNR; green), and unknown (UNK; red) insertions. (E) Percentages of sense-oriented
694 germline and somatic L1Hs insertions in transcripts. The gray line represented the expected
695 proportion if the insertions occurred randomly in both directions. Error bars indicated the 95%
696 confidence intervals.

Supporting Information

Supplementary Figures

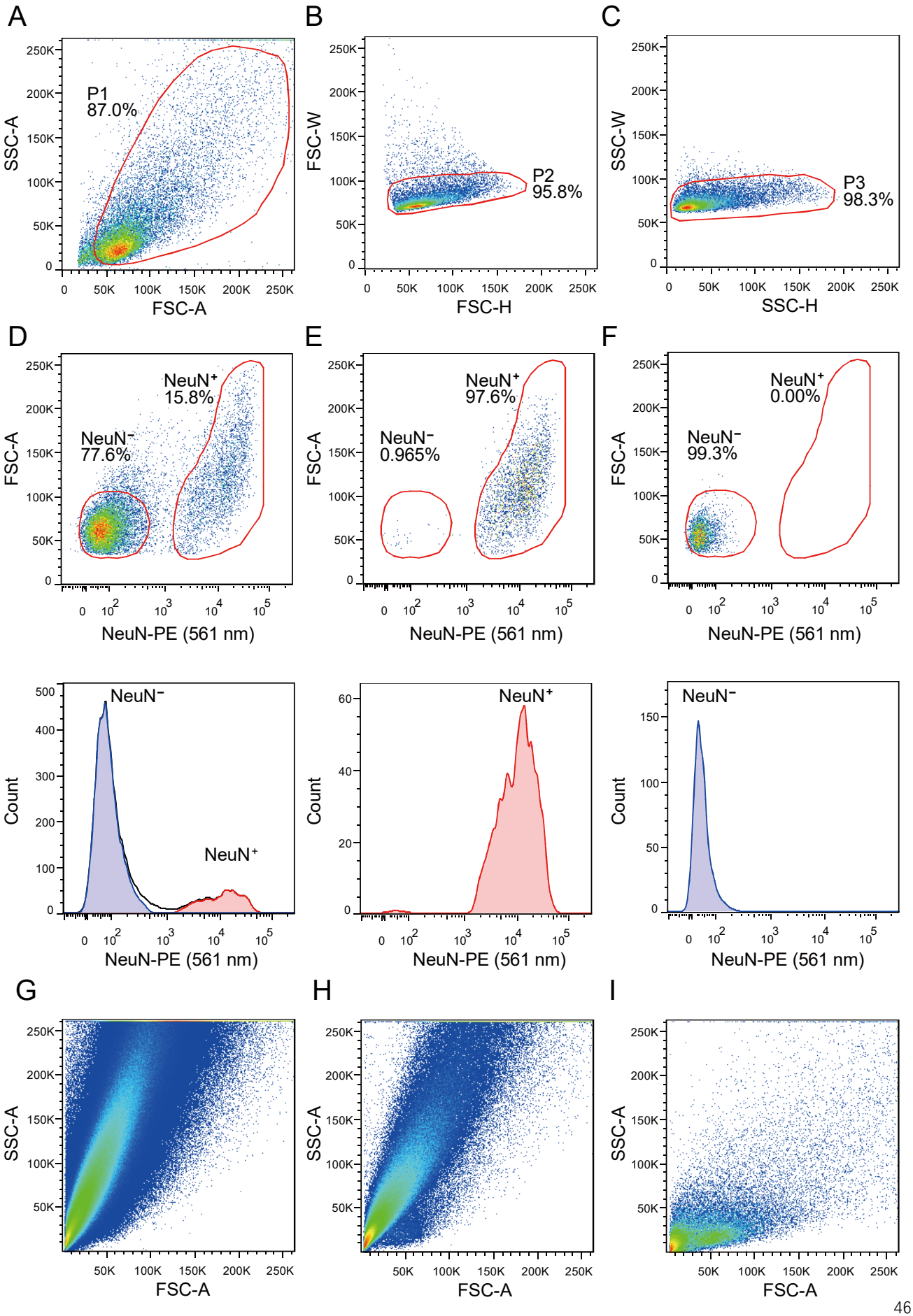
A
P1
87.0%
SSC-A
FSC-A
B
P2
95.8%
FSC-W
FSC-H
C
P3
98.3%
SSC-W
SSC-H
D
NeuN⁺
15.8%
NeuN⁻
77.6%
FSC-A
NeuN-PE (561 nm)
E
NeuN⁺
97.6%
NeuN⁻
0.965%
FSC-A
NeuN-PE (561 nm)
F
NeuN⁺
0.00%
NeuN⁻
99.3%
FSC-A
NeuN-PE (561 nm)
NeuN⁻
NeuN⁺
Count
NeuN-PE (561 nm)
NeuN⁺
Count
NeuN-PE (561 nm)
NeuN⁻
Count
NeuN-PE (561 nm)
G
SSC-A
FSC-A
H
SSC-A
FSC-A
I
SSC-A
FSC-A

699

S1 Fig. Nuclei isolation and NeuN$^+$ fluorescence-activated cell sorting (FACS).

(A)–(D) Purify neuronal nuclei from human PFC. (A) The first gate (P1) was set as an FSC-A vs. SSC-A plot to discriminate the population containing small-size debris. (B)–(C) The second (P2) and third (P3) gates were set as FSC-H vs. FSC-W and SSC-H vs. SSC-D plots, respectively, to remove doublets and clumps. (D) Top: NeuN$^-$ and NeuN$^+$ gates were set in the NeuN-PE (561 nm) vs. FSC-A plot. Bottom: a count plot of NeuN-stained nuclei. (E) Purity analysis of sorted neurons. Top: sorted NeuN$^+$ nuclei were re-analyzed by FACS to confirm the sort purity. Bottom: a count plot of re-analyzed NeuN$^+$ nuclei. (F) Purity analysis of sorted glia. Top: sorted NeuN$^-$ nuclei were re-analyzed by FACS to confirm the sort purity. Bottom: a count plot of re-analyzed NeuN$^-$ nuclei. (G) FSC vs. SSC plot of brain homogenate. Brain homogenate contained a huge amount of cell debris and myelin debris. (H) FSC vs. SSC plot of debris-detached single-nuclei homogenate. Minced brain tissue was soaked overnight before homogenization and then incubated with nonionic detergent, Nonidet P-40, to remove cell debris from nuclear membrane. (I) FSC vs. SSC plot of debris removed nuclei fraction. Cell debris and myelin were separated from nuclei using Percoll density gradient centrifugation.

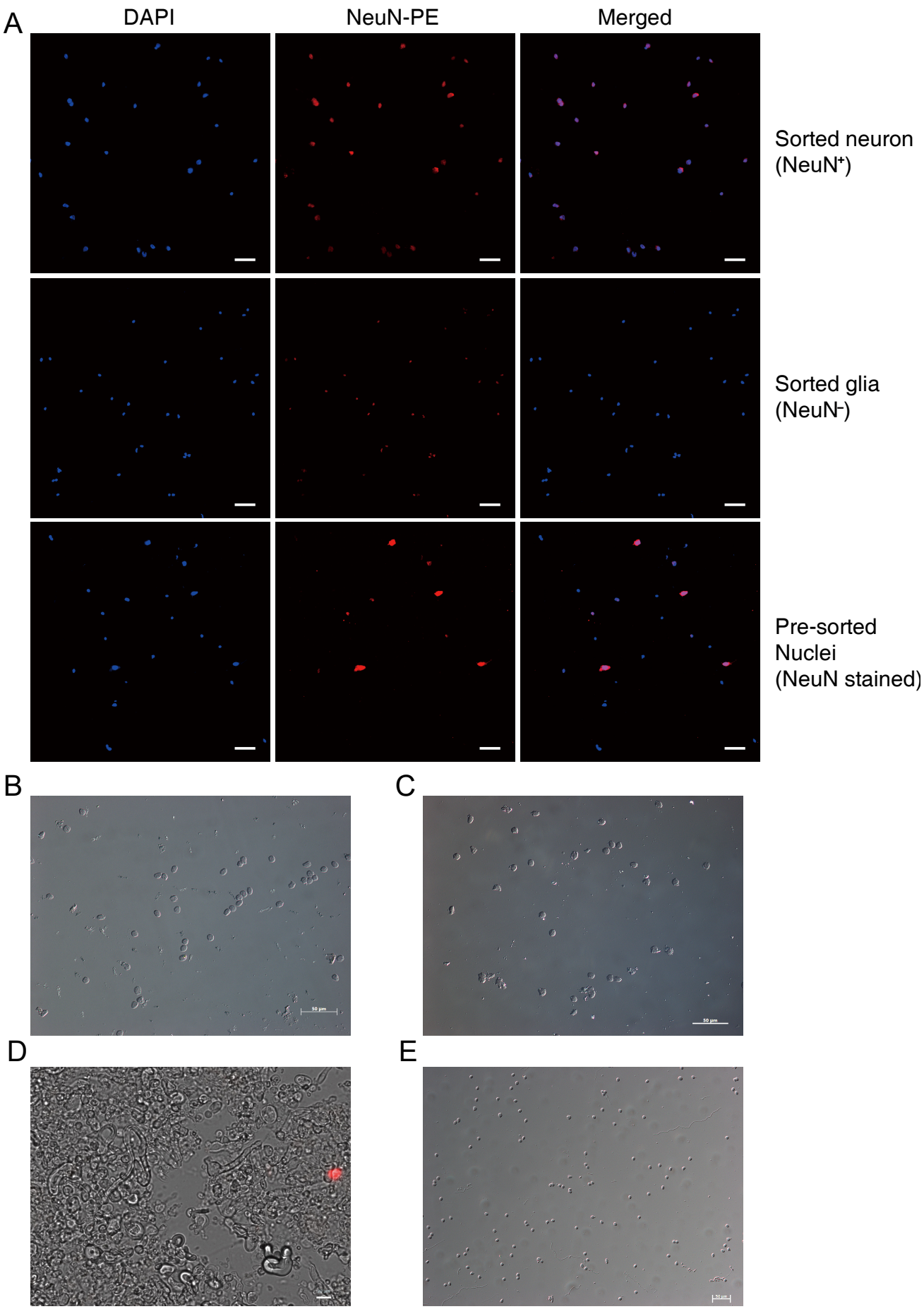
A
DAPI
NeuN-PE
Merged
Sorted neuron
(NeuN+)
Sorted glia
(NeuN-)
Pre-sorted
Nuclei
(NeuN stained)
B
C
D
E

715

716 **S2 Fig. Confirmation of NeuN$^+$ FACS purity and integrity.**

717 (A) Example of fluorescence microscopy confirmation of isolated nuclei. The purity of each fraction
718 was > 95% for NeuN$^+$ and NeuN$^-$ nuclei. Bar = 50 μm. (B)–(C) Examples of integrity confirmation
719 using differential interference contrast (DIC) of sorted neurons (B) and glia (C). Bar = 50 μm. (D)
720 Example of the myelin, lipid, and cell debris layers (12% Percoll) after Percoll density gradient
721 centrifugation. Nuclei were stained with a red fluorescent nuclear counterstain, propidium iodide (PI).
722 Bar = 20 μm. (E) Example of the nuclei fraction layer (35% Percoll) after Percoll density gradient
723 centrifugation. Bar = 50 μm. DAPI, 4',6-diamidino-2-phenylindole; NeuN-PE, PE-conjugated anti-
724 NeuN antibody.

725

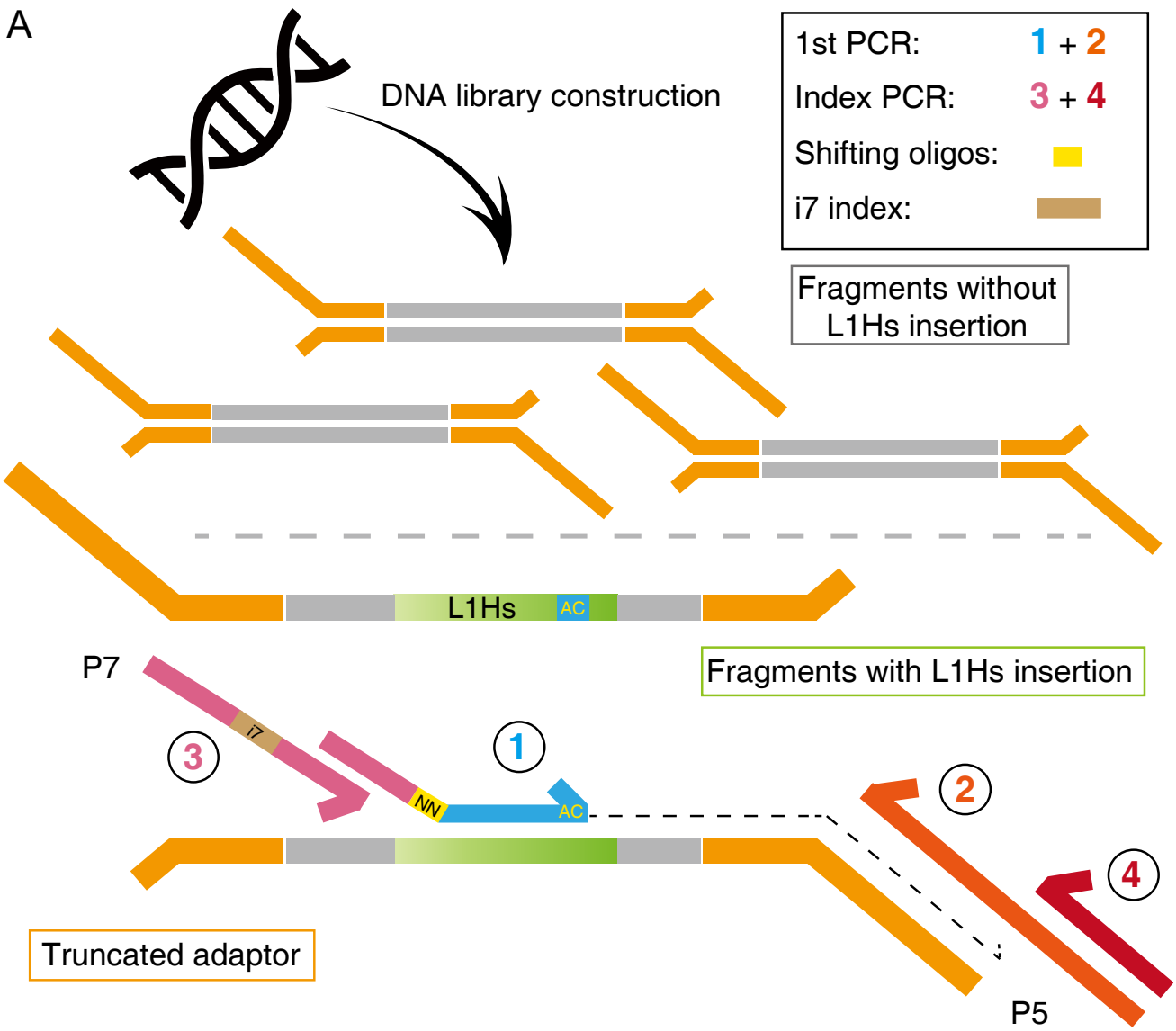
A
DNA library construction
1st PCR: 1 + 2
Index PCR: 3 + 4
Shifting oligos:
i7 index:
Fragments without L1Hs insertion
L1Hs
AC
P7
Fragments with L1Hs insertion
i7
3
1
NN
AC
2
4
Truncated adaptor
P5

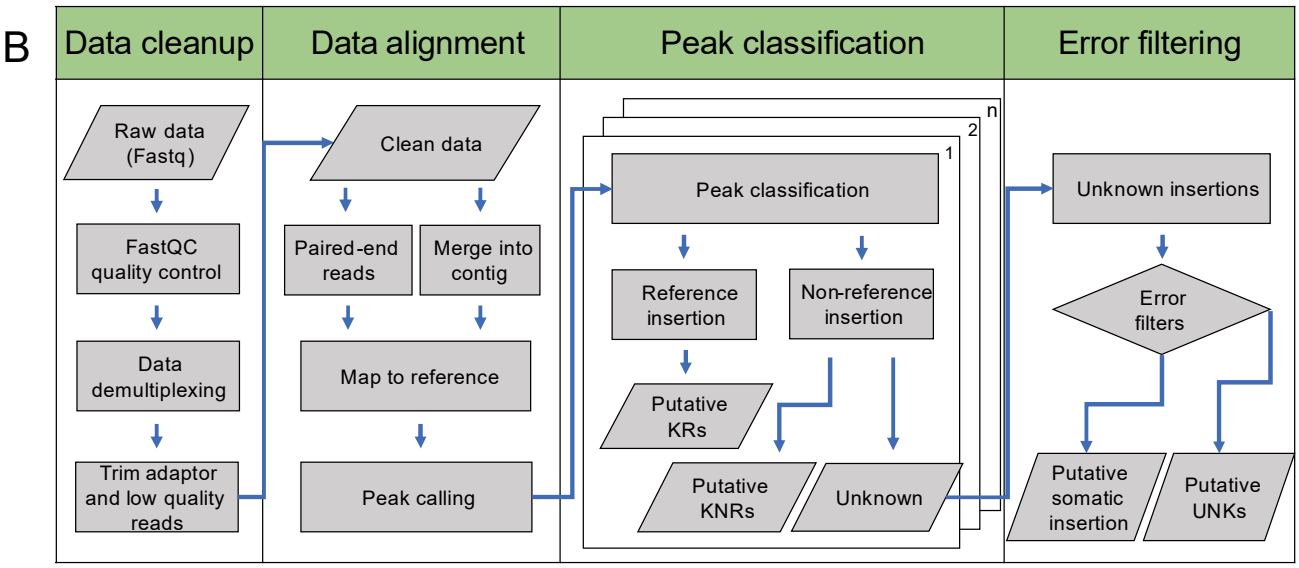
B
Data cleanup
Data alignment
Peak classification
Error filtering
Raw data (Fastq)
FastQC quality control
Data demultiplexing
Trim adaptor and low quality reads
Clean data
Paired-end reads
Merge into contig
Map to reference
Peak calling
n
2
1
Peak classification
Reference insertion
Non-reference insertion
Putative KRs
Putative KNRs
Unknown
Unknown insertions
Error filters
Putative somatic insertion
Putative UNKs

728 **S3 Fig. Schematic diagrams of HAT-seq library construction and computational analysis pipeline.**
729 (A) Schematic of the HAT-seq library construction. After fragmentation, genomic DNA fragments
730 were ligated with P7 truncated adaptors. Adaptor ligated gDNA was used as template for L1Hs
731 amplification PCR. Primers 1 (P7_Ns_L1Hs) was specific to L1Hs diagnostic "AC" motif. See S1
732 Table for primer sequences. (B) Schematic of the HAT-seq data analysis pipeline; full details are
733 provided in the Materials and Methods.
734

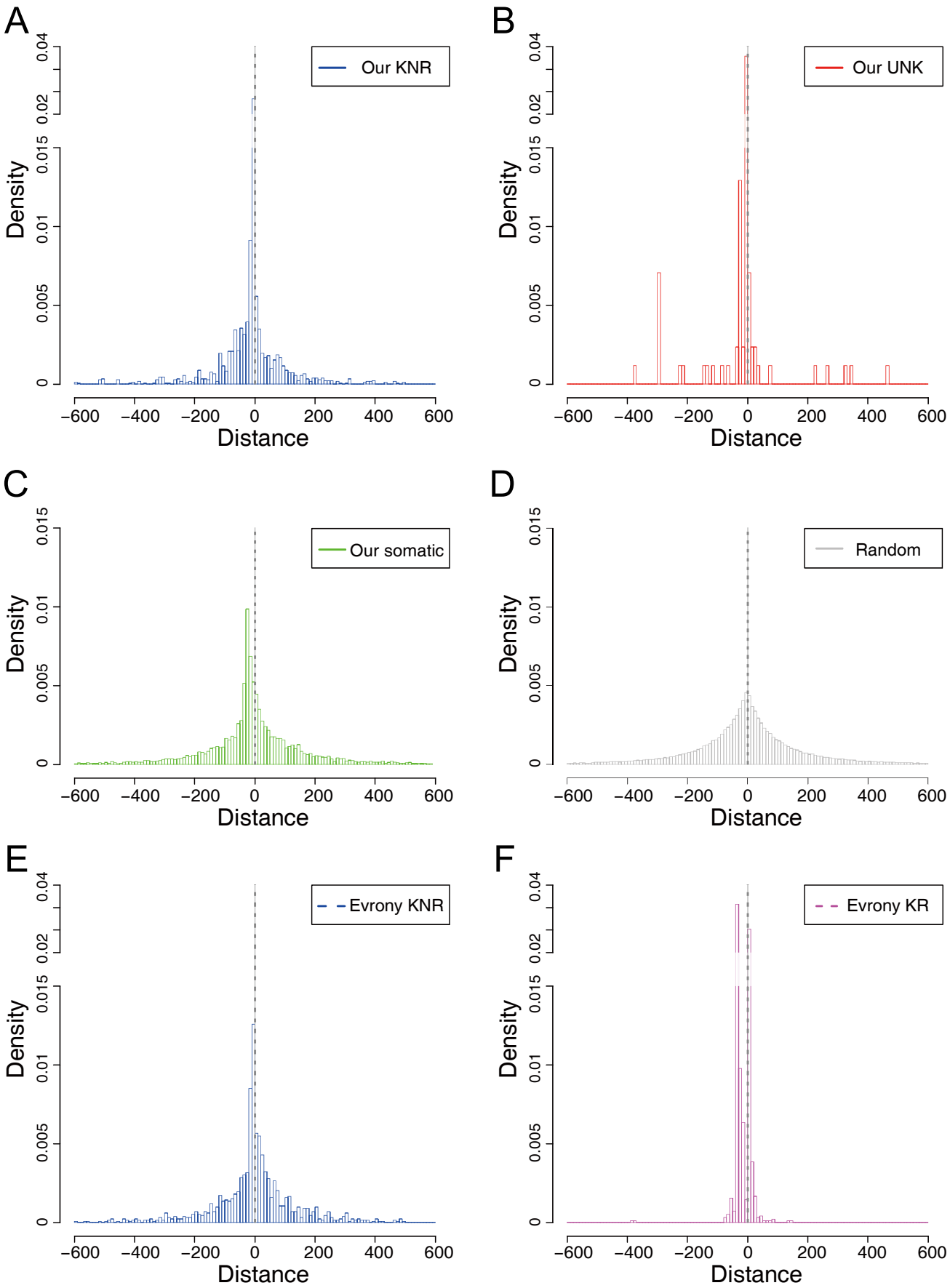
A
Our KNR
Density
Distance
B
Our UNK
Density
Distance
C
Our somatic
Density
Distance
D
Random
Density
Distance
E
Evrony KNR
Density
Distance
F
Evrony KR
Density
Distance

735

736

S4 Fig. EN motif enrichment analysis across all categories of L1Hs insertions.

(A)–(C) The density distributions of L1 EN motifs around germline KNR (A), UNK (B), and somatic L1Hs insertions (C) identified in this study. (D) The random control of the density distributions of L1 EN motifs. (E)–(F) The density distributions of L1 EN motifs around "Evrony KR" and "Evrony KNR" identified in Evrony *et al.* 2012. The bin size of histogram was 10bp. L1 EN motifs included seven specific motifs (TTAAAA, TTAAGA, TTAGAA, TTGAAA, TTAAAG, CTAAAA, TCAAAA).

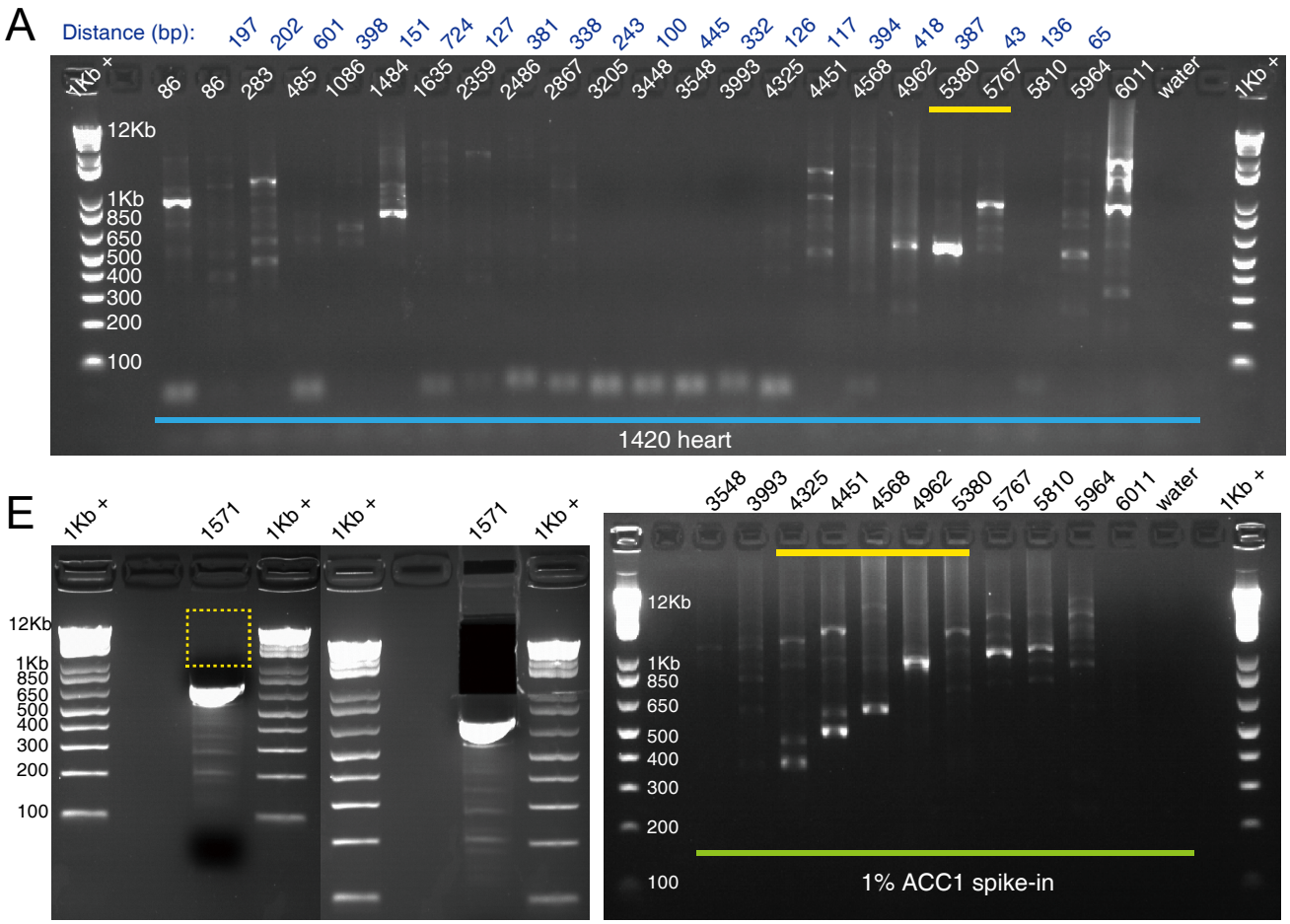
A
Distance (bp): 197 202 601 398 151 724 127 381 338 243 100 445 332 126 117 394 418 387 43 136 65
1Kb + 86 86 283 485 1086 1484 1635 2359 2486 2867 3205 3448 3548 3993 4325 4451 4568 4962 5380 5767 5810 5964 6011 water 1Kb +
12Kb
1Kb
850
650
500
400
300
200
100
1420 heart
E
1Kb + 1571 1Kb + 1Kb + 1571 1Kb +
12Kb
1Kb
850
650
500
400
300
200
100
3548 3993 4325 4451 4568 4962 5380 5767 5810 5964 6011 water 1Kb +
12Kb
1Kb
850
650
500
400
300
200
100
1% ACC1 spike-in

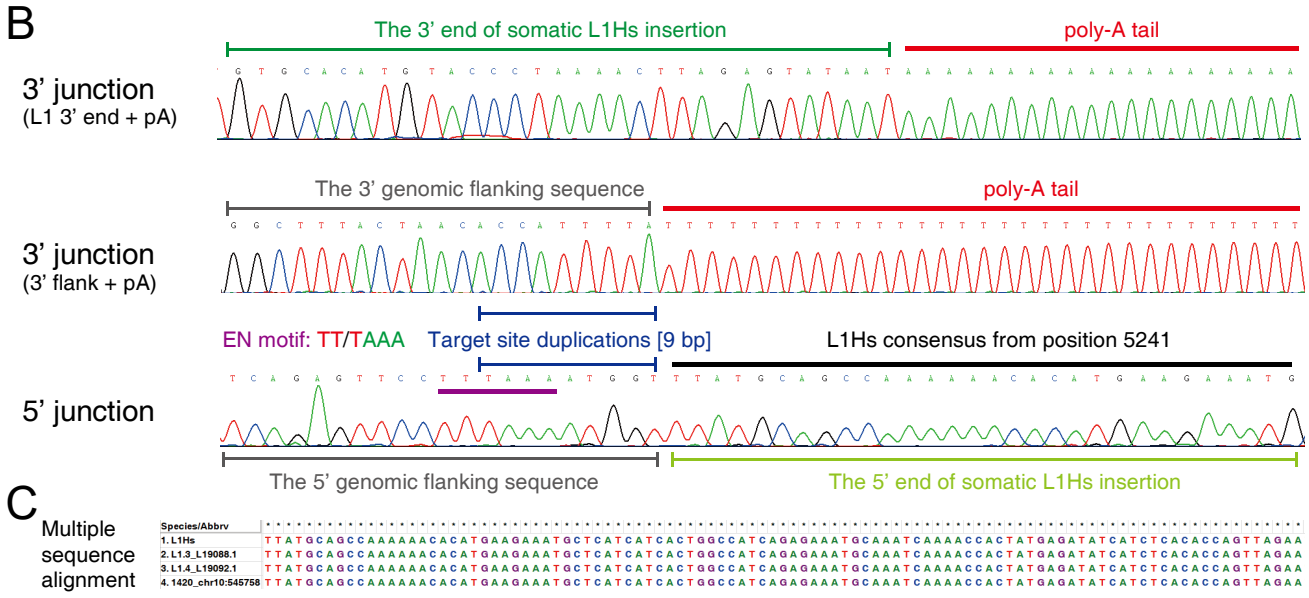
B
The 3' end of somatic L1Hs insertion
poly-A tail
3' junction
(L1 3' end + pA)
The 3' genomic flanking sequence
poly-A tail
3' junction
(3' flank + pA)
EN motif: TT/TAAA
Target site duplications [9 bp]
L1Hs consensus from position 5241
5' junction
The 5' genomic flanking sequence
The 5' end of somatic L1Hs insertion
C
Multiple sequence alignment
Species/Abbrv
1. L1Hs
2. L1.3_L19088.1
3. L1.4_L19092.1
4. 1420_chr10:545758

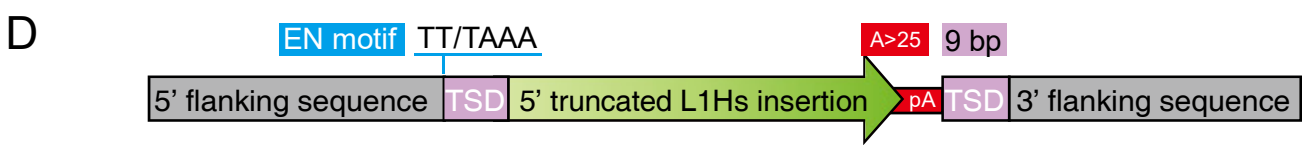
D
EN motif
TT/TAAA
A>25
9 bp
5' flanking sequence
TSD
5' truncated L1Hs insertion
pA
TSD
3' flanking sequence

746 **S5 Fig. A 5' truncated heart-specific L1Hs insertion in a Rett patient.**

747 (A) The agarose gel image of 5' junction nested PCR validation for the heart-specific L1Hs insertion
748 in the Rett patient (UMB#1420). The location of primers used in 5' junction PCR assays were labeled
749 on the top of each lane. The distances between each primer pairs were labeled on the top (dark blue).
750 The blue line indicated that the heart gDNA from UMB#1420 was used as template. The green line
751 indicated the positive control assays where 1% ACC1 spike-in gDNA was used as template and the 5'
752 junction of a heterozygous, ~2Kb L1Hs insertion (ACC1_60) was amplified by 5' junction nested PCR
753 assays (S11 Table and Appendix 4). The yellow line indicated stair-step bands with expected distance
754 between each pair of 5' PCR reactions. 1Kb +: 1 Kb Plus DNA ladder. (B) The Sanger sequencing
755 chromatograms of the 3' and 5' junctions of somatic insertion (1420_chr10:545758). Top: the 3'
756 junction of L1Hs insertion including the 3' end of L1Hs element and its poly-A tail. Middle: the poly-A
757 tail and 3' flanking genomic sequence of L1Hs insertion. Bottom: the 5' junction of L1Hs insertion
758 including the 5' end of L1Hs elements and its 5' flanking genomic sequence. The purple line indicated
759 the sequence of the L1 EN motif. The blue lines indicated the sequence of TSDs. (C) The multiple
760 sequence alignment. Sequence set included the 5' junction sequence of somatic L1Hs insertion
761 (1420_chr10:545758) and three L1Hs consensus sequences (L1Hs Repbase consensus and two hot L1s
762 in human [L1.3 and L1.4]). (D) The schematic structure of the highly 5' truncated (~800 bp),
763 heart-specific L1Hs insertion in the Rett patient (UMB#1420). (E) Agarose gel images of full-length
764 PCR for the somatic L1Hs insertion (1571_chr3:2944507). Yellow rectangle indicated the cut region
765 above the "empty site" band of insertion. gDNA eluted from gel extraction was used as the template
766 for downstream 5' junction PCR. 1Kb +: 1 Kb Plus DNA ladder.

767

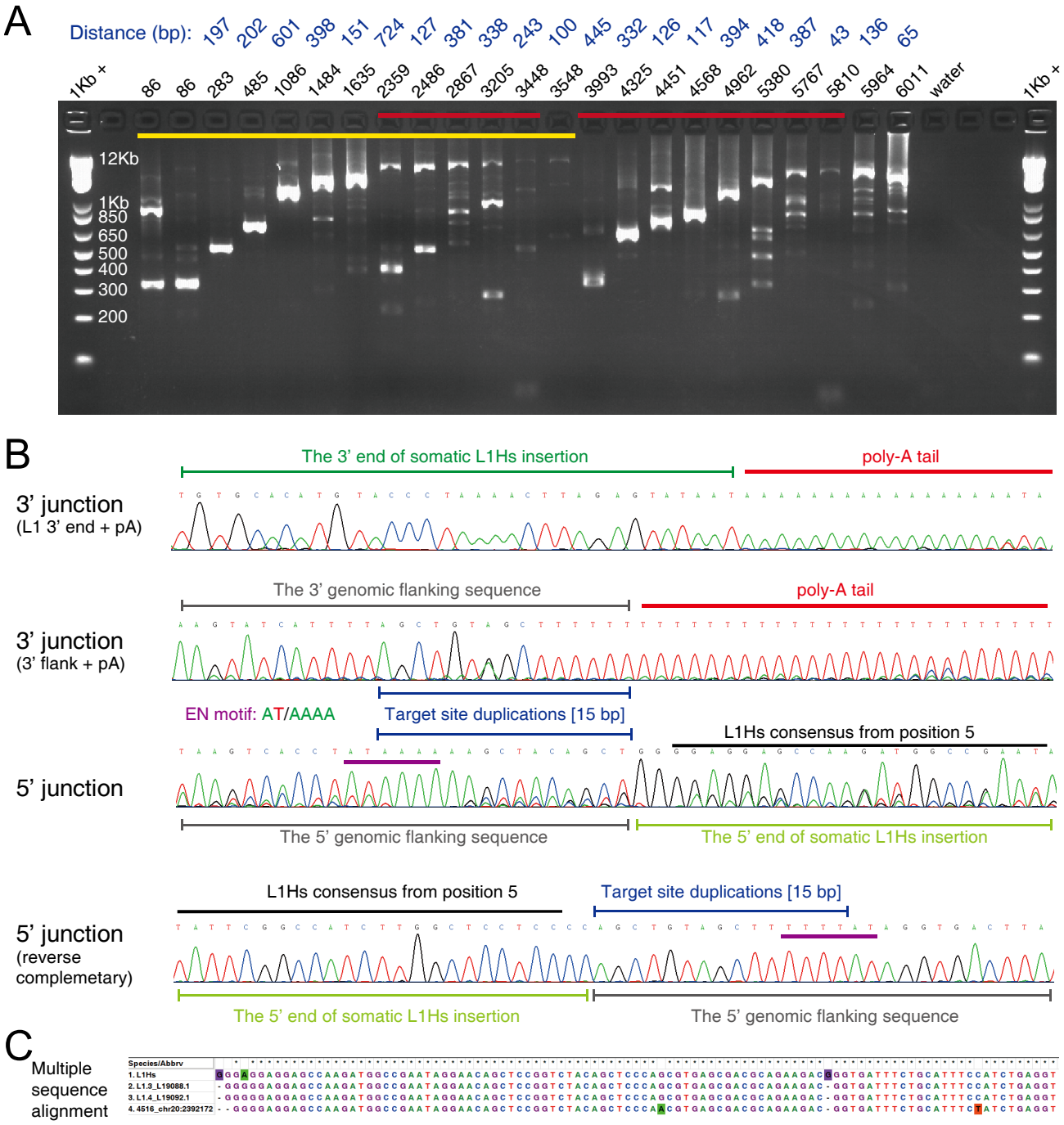
A
Distance (bp): 197 202 601 398 151 724 127 381 338 243 100 445 332 126 117 394 418 387 43 136 65
1Kb + 86 86 283 485 1086 1484 1635 2359 2486 2867 3205 3448 3548 3993 4325 4451 4568 4962 5380 5767 5810 5964 6011 water 1Kb +
12Kb
1Kb
850
650
500
400
300
200
B
The 3' end of somatic L1Hs insertion
poly-A tail
3' junction
(L1 3' end + pA)
The 3' genomic flanking sequence
poly-A tail
3' junction
(3' flank + pA)
EN motif: AT/AAAA
Target site duplications [15 bp]
L1Hs consensus from position 5
5' junction
The 5' genomic flanking sequence
The 5' end of somatic L1Hs insertion
L1Hs consensus from position 5
Target site duplications [15 bp]
5' junction
(reverse
complemetary)
The 5' end of somatic L1Hs insertion
The 5' genomic flanking sequence
C
Multiple
sequence
alignment
Species/Abbrv
1. L1Hs
2. L1.3_L19088.1
3. L1.4_L19092.1
4. 4516_chr20:2392172
D
EN motif
AT/AAAA
A>40
15 bp
5' flanking sequence
TSD
somatic full-length L1Hs insertion
pA
TSD
3' flanking sequence

S6 Fig. A full-length embryonic somatic L1Hs insertion in a Rett patient.

(A) The agarose gel image of 5' junction nested PCR validation for the embryonic somatic L1Hs insertion (4516_chr20:2392172) in the Rett patient (UMB#4516). The location of primers used in 5' junction PCR assays were labeled on the top of each lane. The distances between each primer pairs were labeled on the top (dark blue). The yellow line indicated stair-step bands with expected distance between each pair of 5' PCR reactions. The red lines indicated false positive stair-step bands that were resulted from non-specific amplification of L1PA subfamilies. 1Kb +: 1 Kb Plus DNA ladder. (B) The Sanger sequencing chromatograms of the 3' and 5' junctions of somatic insertion (4516_chr20:2392172). Top: the 3' junction of L1Hs insertion including the 3' end of L1Hs element and its poly-A tail. Middle-upper: the poly-A tail and 3' flanking genomic sequence of L1Hs insertion. Middle-lower: the 5' junction of L1Hs insertion including the 5' end of L1Hs elements and its 5' flanking genomic sequence. The nucleotides shifted chromatogram was resulted from the DNA polymerase slippage at homopolymers in the upstream region (L1MB3 element). Bottom: the reverse complementary sequence of the 5' junction of L1Hs insertion. The purple lines indicated the sequence of the L1 EN motif. The blue lines indicated the sequence of TSDs. (C) The multiple sequence alignment. Sequence set included the 5' junction sequence of somatic L1Hs insertion (4516_chr20:2392172) and three L1Hs consensus sequences (L1Hs Repbase consensus and two hot L1s in human [L1.3 and L1.4]). (D) The schematic structure of the full-length, embryonic somatic L1Hs insertion in the Rett patient (UMB#4516).

A

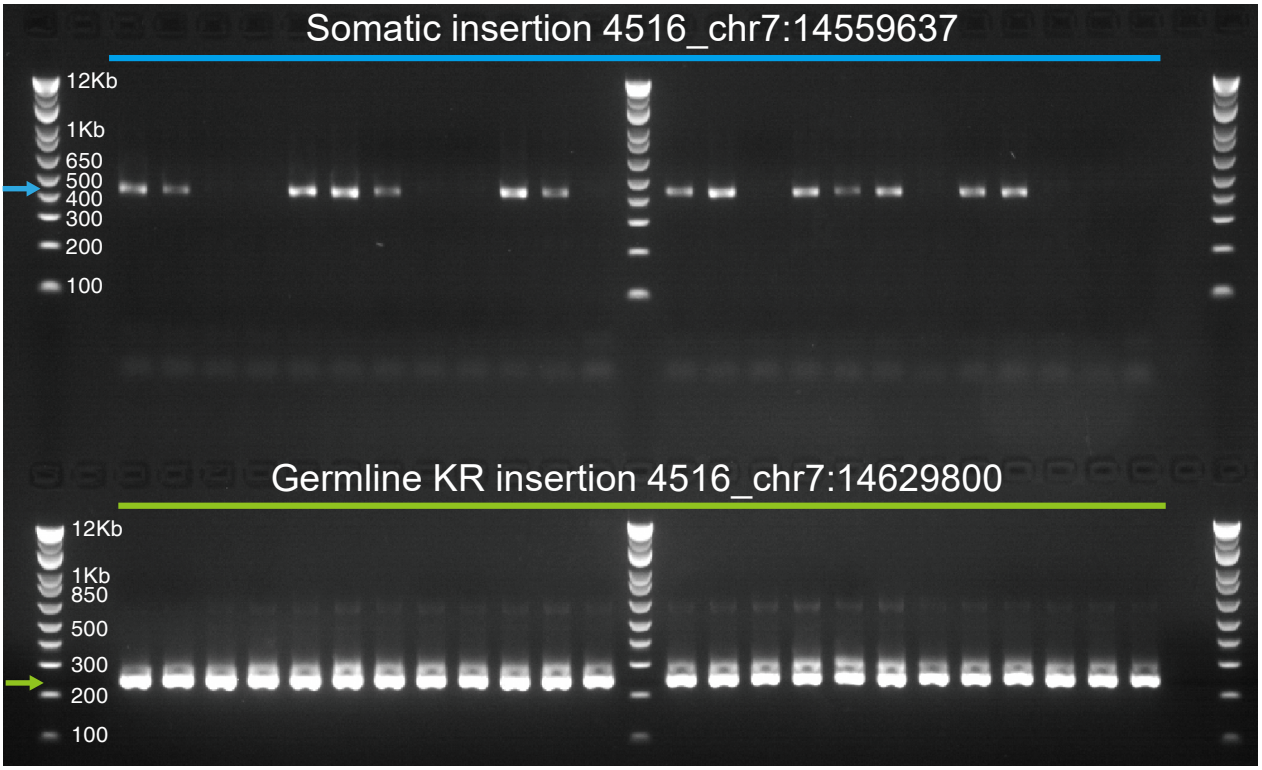
Somatic insertion 4516_chr7:14559637
12Kb
1Kb
650
500
400
300
200
100
Germline KR insertion 4516_chr7:14629800
12Kb
1Kb
850
500
300
200
100

B

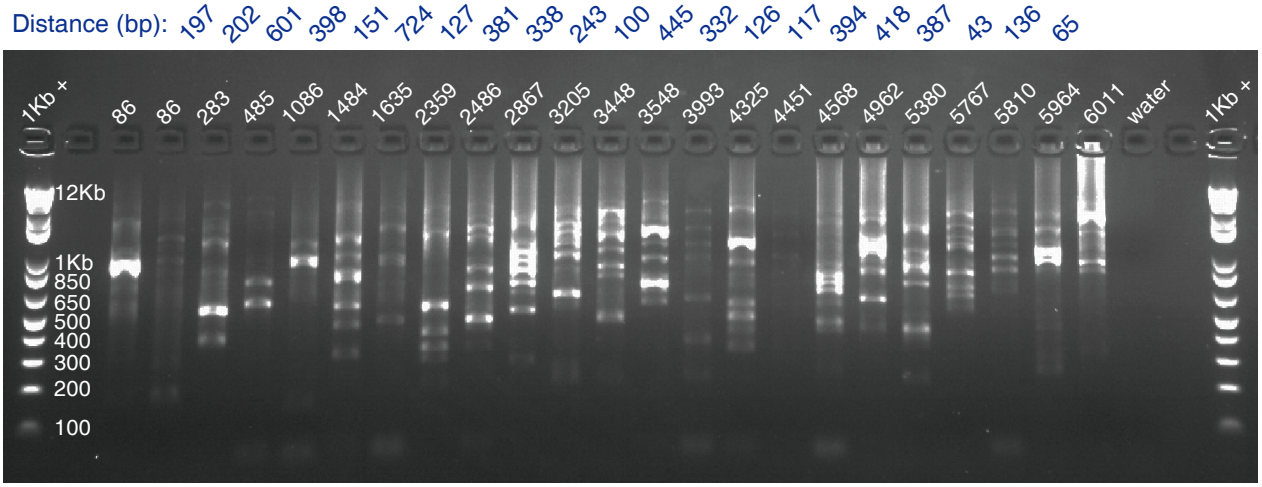
Distance (bp): 197 202 601 398 151 724 127 381 338 243 100 445 332 126 117 394 418 387 43 136 65
1Kb +
86
86
283
485
1086
1484
1635
2359
2486
2867
3205
3448
3548
3993
4325
4451
4568
4962
5380
5767
5810
5964
6011
water
1Kb +
12Kb
1Kb
850
650
500
400
300
200
100

790
791

792 **S7 Fig. An embryonic somatic L1Hs insertions in a Rett patient.**

793 (A) The occupancy of the embryonic somatic L1Hs insertion (4516_chr7:14559637) in digital nested
794 3' PCR assays. As chr7:14559637 had been validated by 3' nested PCR (Fig 3H), we assumed its
795 mosaicism > 0.1%. Then, DNA sample was diluted to a target somatic insertion concentration of 0.3
796 copies/μL/well. The chr7:14559637 insertion showed a 58.3% (14/24) occupancy (corresponds to
797 ~0.2% mosaicism), compared to 100% occupancy yielded by germline KR insertion control
798 (chr7:14629800) from the same donor. Blue and green arrows indicated the band with target size. (B)
799 The agarose gel image of 5' junction nested PCR validation for the embryonic somatic L1Hs
800 insertion (4516_chr7:14559637) in the Rett patient (UMB#4516). The location of primers used in 5'
801 junction PCR assays were labeled on the top of each lane. The distances between each primer pairs
802 were labeled on the top (dark blue). No stair-step bands with expected distance was observed,
803 suggesting that the somatic L1Hs insertion (4516_chr7:14559637) might harbor a 5' inversion. 1Kb
804 +: 1 Kb Plus DNA ladder.

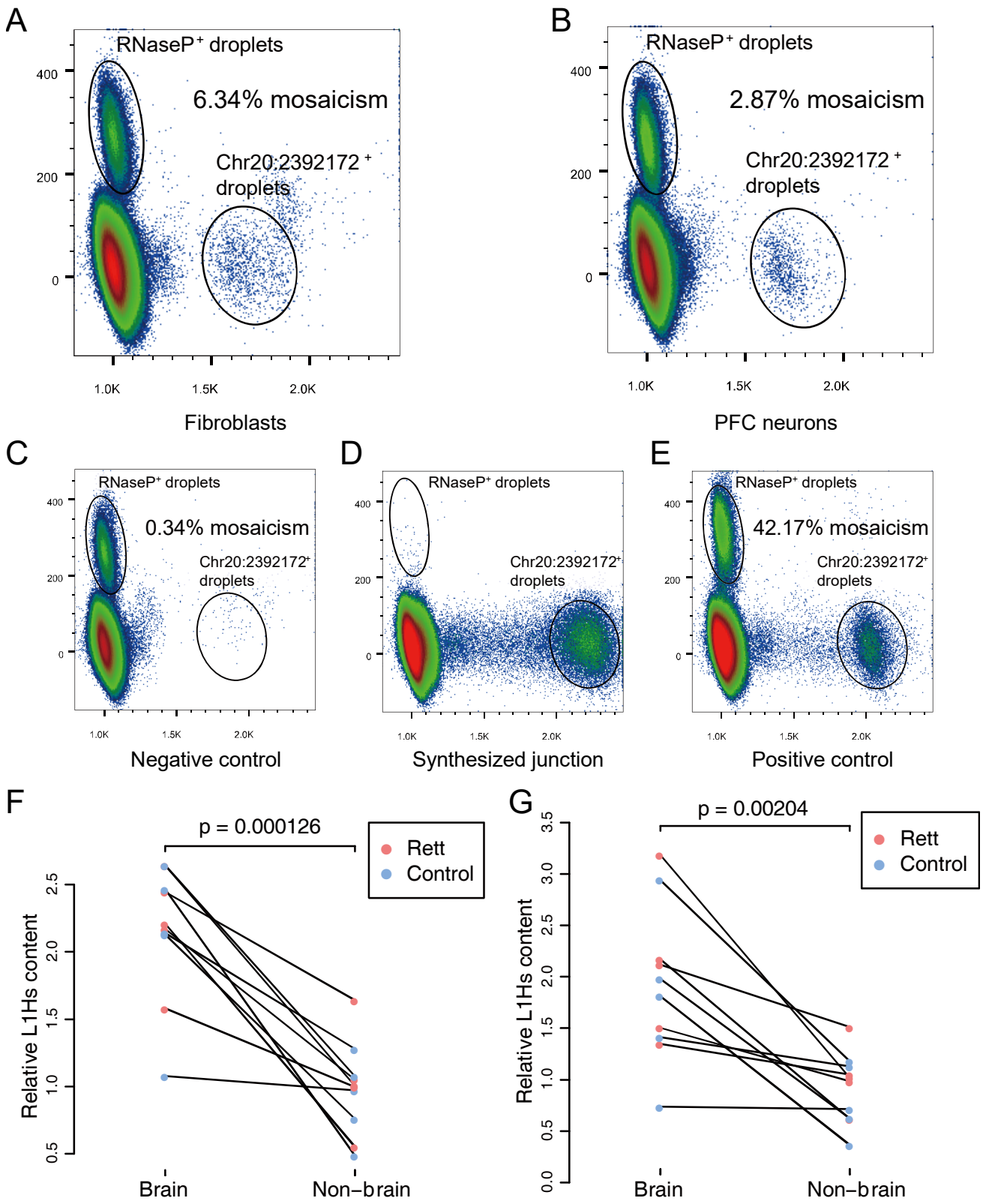
A
RNaseP⁺ droplets
6.34% mosaicism
Chr20:2392172⁺ droplets
Fibroblasts
B
RNaseP⁺ droplets
2.87% mosaicism
Chr20:2392172⁺ droplets
PFC neurons
C
RNaseP⁺ droplets
0.34% mosaicism
Chr20:2392172⁺ droplets
Negative control
D
RNaseP⁺ droplets
Chr20:2392172⁺ droplets
Synthesized junction
E
RNaseP⁺ droplets
42.17% mosaicism
Chr20:2392172⁺ droplets
Positive control
F
p = 0.000126
Rett
Control
Relative L1Hs content
Brain
Non−brain
G
p = 0.00204
Rett
Control
Relative L1Hs content
Brain
Non−brain

807 **S8 Fig. Qualitative and quantitative analysis of L1Hs insertions.**

808 (A)–(E) Droplet digital PCR (ddPCR) assays to quantify mosaicism (percentage of cells) of somatic
809 L1Hs insertions at chr20:2392172 in fibroblasts (A) and PFC neurons (B) from Rett patient
810 UMB#4516. Fragmented ACC1 blood gDNA was used as template for negative control assay (C). A
811 mixed template containing fragmented ACC1 blood gDNA and diluted synthesized L1Hs genome
812 junction oligos (D) was used for positive control assay (E). RNaseP served as a genomic copy number
813 reference (copy number = 2). L1Hs and RNaseP assays were labeled with FAM and VIC, respectively.
814 (F)–(G) Relative somatic L1Hs content in PFC neurons and non-brain tissue from the same donor,
815 normalized by the read count of KRs (F) or UNKs (G) from the same tissue sample.
816

817 **Supplementary Tables**

818

819 **S1 Table. Primer sequences of HAT-seq library**

820

821 **S2 Table. ACC1-specific insertions and statistics of positive controls**

822

823 **S3 Table. Statistics of error filters**

824

825 **S4 Table. Clinical characterization of patients with Rett syndrome**

826

827 **S5 Table. Statistics of HAT-seq libraries**

828

829 **S6 Table. Statistics of known reference insertions among all samples**

830

831 **S7 Table. Statistics of polymorphic insertions among all samples**

832

833 **S8 Table. Statistics of somatic insertions among all samples**

834

835 **S9 Table. TPRT hallmarks annotation for all somatic insertions**

836

837 **S10 Table. 3' junction nested PCR and digital droplet PCR validation**

838

S11 Table. 5' junction nested PCR validation

S12 Table. Annotation for somatic exonic insertions

S13 Table. Raw data for statistical analyses

S14 Table. Quantification statistics among all samples

S15 Table. L1Hs enrichment analysis on HAT-seq

S16 Table. 3' junction PCR validation for germline insertions

851 **Supplementary Files**

852

853 **Appendix 1. Cell type-specific sorting by BD Aria II using postmortem human brain sample**

854

855 **Appendix 2. Identification of ACC1-specific insertion and their zygosity**

856

857 **Appendix 3. Detection of somatic L1Hs insertions at low levels in spike-in HAT-seq libraries**

858

859 **Appendix 4. Benchmarking PCR validation assays for low-frequency somatic insertions**

860

861 **Appendix 5. Experimental validation of polymorphic germline L1Hs insertions**